

Fast variable selection for distributional regression with application to continuous glucose monitoring data

Alexander Coulter Rashmi N. Aurora Naresh M. Punjabi Irina Gaynanova	<i>Department of Statistics, Texas A&M University</i> <i>Grossman School of Medicine, New York University</i> <i>Miller School of Medicine, University of Miami</i> <i>Department of Biostatistics, University of Michigan</i>
---	---

March 5, 2024

Abstract

With the growing prevalence of diabetes and the associated public health burden, it is crucial to identify modifiable factors that could improve patients' glycemic control. In this work, we seek to examine associations between medication usage, concurrent comorbidities, and glycemic control, utilizing data from continuous glucose monitors (CGMs). CGMs provide high-frequency interstitial glucose measurements, but reducing data to simple statistical summaries is common in clinical studies, resulting in substantial information loss. Recent advancements in the Fréchet regression framework allow to utilize more information by treating the full distributional representation of CGM data as the response, while sparsity regularization enables variable selection. However, the methodology does not scale to large datasets. Crucially, variable selection inference using subsampling is computationally infeasible. We develop a new algorithm for sparse distributional regression by deriving a new explicit characterization of the gradient and Hessian of the underlying objective function, while also utilizing rotations on the sphere to perform feasible updates. The updated method is up to 10000+ fold faster than the original approach, opening the door for applying sparse distributional regression to large-scale datasets and enabling previously unattainable subsampling-based inference. Applying our method to CGM data from patients with type 2 diabetes and obstructive sleep apnea, we found a significant association between sulfonylurea medication and glucose variability without evidence of association with glucose mean. We also found that overnight oxygen desaturation variability showed a stronger association with glucose regulation than overall oxygen desaturation levels.¹

1 Introduction

Diabetes mellitus is a chronic illness characterized by elevated glucose levels. Type 1 diabetes results from an autoimmune destruction of the pancreas' beta cells which are responsible for the production of insulin. In contrast, type 2 diabetes is characterized by a state of insulin resistance which is accompanied by a decrease in insulin production. Diabetes is a leading cause of death among U.S. adults ([Ahmad et al., 2023](#)) and is linked to development of various complications ([Sobrin et al., 2011](#); [Resnick and Howard, 2002](#); [Moxey et al., 2011](#); [Kodl and Seaquist, 2008](#)). While diabetes-related mortality has fallen in recent decades ([Callaghan et al., 2020](#)) due to improvements in treatment and interventions ([Jonas et al., 2021](#); [Rosenquist and Fox, 2018](#)), the growing diabetes prevalence ([CDC, 2023](#)) and the associated public health burden make it crucial to identify modifiable factors that could improve patients' glycemic control.

In this work, we seek to examine associations between medication usage, obstructive sleep apnea (OSA) and glycemic control. OSA is a sleep-related disorder characterized by cessation of breathing during sleep, and has a high estimated prevalence (54%-86%) among patients with type 2 diabetes ([Singh et al., 2021](#); [Lam et al., 2010](#); [Foster et al., 2009](#)). Our major motivating application is "Hyperglycemic Profiles in Obstructive

¹Keywords: Diabetes, Fréchet Regression, Gradient Descent, Optimization, Sleep Apnea, Stability Selection

Sleep Apnea (HYPNOS)” study (Rooney et al., 2021), which aimed to characterize the effects of positive airway pressure (PAP) therapy in patients with OSA and concurrent type 2 diabetes. For each patient, interstitial glucose levels were recorded via Dexcom G4 continuous glucose monitor (CGM), which has a measurement frequency of 5 minutes with an average of 10 days of data per patient. Herein, our goal is to quantify the association between patient characteristics and glycemic control based on CGM data at baseline (before the institution of PAP therapy). The effects of patients’ medication usage and degree of OSA severity are of particular interest, considering the range of available medication types and the possibility of treating OSA with PAP therapy. Given a large number of available medication types, demographic characteristics and measures of OSA severity, we are interested in performing data-driven variable selection and inference with CGM data serving as response.

In clinical practice, it’s common to reduce CGM data to crude summaries (e.g., mean, time-in-range), and subsequently evaluate the effect of specific covariates on those summaries (Battelino et al., 2022). However, a large number of available summaries (40+) makes it difficult to discern which are most appropriate in a given context (Gaynanova, 2022). Utilization of all summary measures leads to the loss of statistical power due to the necessity of multiple comparisons adjustment. Functional data analysis (FDA) (Wang et al., 2016) provides an alternative approach by treating the entire CGM profile as a functional response. However, due to misalignment of CGM profiles across patients (due to differences in time the sensor is worn, meal intake, physical activity, and sleep patterns), FDA applications are either restricted to time periods less confounded by environmental factors (e.g., sleep time in Gaynanova et al. (2022); Sergazinov et al. (2023)), or are based on aggregated data over 24h domain (Law et al., 2015; Scott et al., 2020). As a consequence, despite numerous studies identifying associations between OSA and glucose metabolism (Punjabi et al., 2002; Lindberg et al., 2012), the effects of OSA severity on glycemic control are not well elucidated, remaining an open area of study (Reutrakul and Mokhlesi, 2017). In the context of HYPNOS study, initial analysis using CGM summaries post randomization failed to elucidate the effects of PAP therapy on glycemic metrics (Aurora et al., 2022). Without advancements in algorithms that provide better characterization of temporal features of CGM data, the adverse effects of OSA on glucose metabolism will likely remain underappreciated.

Distributional analysis provides an alternative framework for CGM data as it advances on traditional summaries by using the whole distribution function of glucose levels (Matabuena et al., 2021; Petersen et al., 2022), while avoiding time alignment issues in FDA methods. Figure 1 illustrates the full CGM profile of one selected study participant, with corresponding distributional representation via histogram and empirical quantile function. Recent advancements in the Fréchet regression framework (Petersen and Müller, 2019) allow to treat the full distributional representation of CGM data as the response, while sparsity regularization as in Tucker et al. (2023) enables variable selection as is the goal in our study. However, the original methodology does not scale to large datasets. In our application with sample size $n = 207$, covariate dimension $p = 34$ and a sequence of 20 sparsity tuning parameters, the original method took approximately 1.5 hours on a standard laptop. While this model fitting step is still feasible on our data, albeit slow, it is not feasible for data with hundreds of covariates or data from population-scale cohorts. For example, distributional approaches are also advantageous for data from actigraphy devices (Ghosal et al., 2021; Matabuena and Petersen, 2023), while large-scale repositories, such as UK Biobank (Doherty et al., 2017), contain both actigraphy data and large number of individual’s characteristics. Currently, sparse distributional regression cannot be applied to such large-scale studies. More crucially, the associated computing costs of model fitting make it infeasible to perform variable selection inference using subsampling-based techniques, such as stability selection (Meinshausen and Bühlmann, 2010), even on our data.

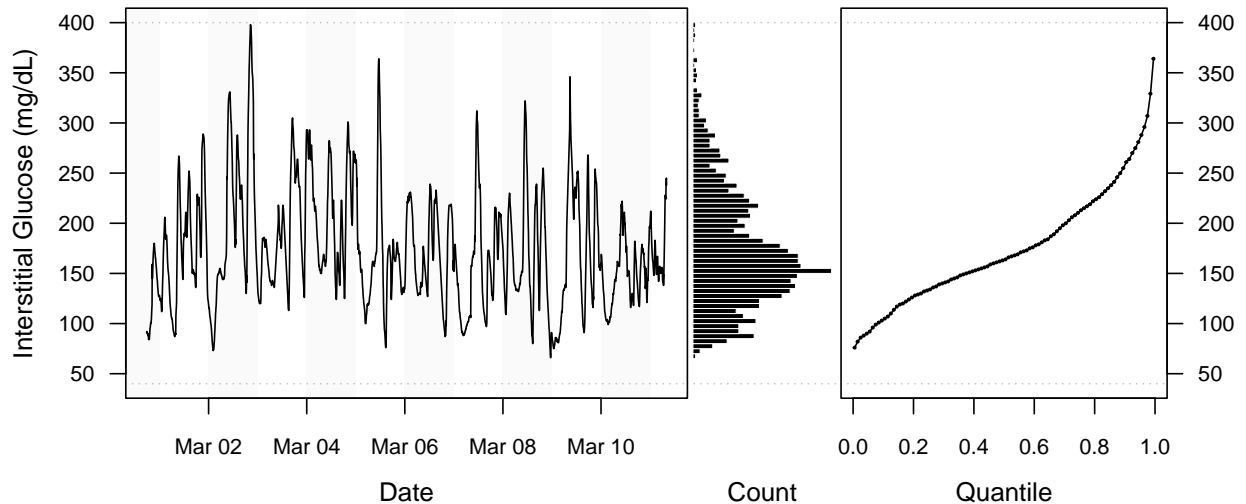


Figure 1: CGM profile (*left*) of a selected subject from HYPNOS study, represented via histogram (*center*) and empirical quantile function (*right*).

In light of our scientific goal to perform variable selection with inference on HYPNOS data, our main innovation is in developing a new algorithm to enable the application of the sparse distributional regression methodology on a large scale. From the statistical perspective, variable selection with Fréchet regression (Tucker et al., 2023) leverages an assumption that only a subset of covariates is relevant for the prediction of distributional response. From the optimization perspective, this assumption translates into estimating a vector $\hat{\boldsymbol{\lambda}} \in \mathbb{R}^p$ with a simplex constraint, where either $\hat{\lambda}_k > 0$ (the k^{th} covariate is selected) or $\hat{\lambda}_k = 0$ (the k^{th} covariate is not selected), leading to highly non-trivial embedded optimization problem with constraints. The existing approach is based on updating one element of $\boldsymbol{\lambda}$ at a time, making it challenging to scale the approach to settings with many covariates. Furthermore, the existing algorithm does not take advantage of the gradient information, which we believe is due to associated difficulties in characterizing the gradient. Our proposed algorithm is methodologically new in several ways: (i) we obtain closed-form characterization of the gradient and Hessian for distributional responses by taking advantage of the optimality conditions of the embedded problem, thus enabling the use of gradient-based methods; (ii) we replace $\hat{\boldsymbol{\lambda}}$'s simplex constraint with a spherical constraint, thus enabling feasible updates of the whole vector $\boldsymbol{\lambda}$ by performing rotation steps in the directions against the gradient. The resulting geodesic gradient descent is 10,000+ folds faster than the original approach. Crucially, it allows us to perform variable selection inference for our scientific study via stability selection (Meinshausen and Bühlmann, 2010); such inference was previously computationally infeasible.

In summary, our contributions are the following:

1. We develop a new algorithm for sparse distributional regression that opens the door to applying the methodology to large-scale datasets;
2. We combine our algorithm with stability selection to enable previously unattainable variable selection inference within sparse distributional regression framework;
3. In the analysis of HYPNOS data, we find a significant association between sulfonylurea medication and glucose variability without evidence of association with glucose mean. We also find that overnight oxygen desaturation variability shows a stronger association with glucose regulation than overall oxygen

desaturation levels.

The rest of the paper is organized as follows. Section 2 describes the HYPNOS data and relevant scientific questions. Section 3 reviews Fréchet regression with variable selection. Section 4 provides development of the proposed algorithm. Section 5 describes stability selection for inference. Section 6 evaluates performance on synthetic data. Section 7 describes the application to HYPNOS data. Section 8 concludes with discussion.

Notation. For a matrix $\mathbf{A} = (a_{i,j}) \in \mathbb{R}^{n \times m}$, let $\mathbf{A}_j = (a_{1,j} \dots a_{n,j})^\top$ be its j^{th} column, and $\mathbf{a}_i = (a_{i,1} \dots a_{i,m})^\top$ its i^{th} row; let $\|\mathbf{A}\|_F^2 = \sum_{i,j} a_{i,j}^2$; let \mathbf{A}^- be a generalized inverse of \mathbf{A} ; let \mathbf{A}_+ be the positive part of \mathbf{A} , i.e. $(a_{i,j})_+ = \max\{a_{i,j}, 0\}$; and let $\mathbb{P}_{\mathbf{A}}$ be the orthogonal projector onto the column space of \mathbf{A} . For two matrices \mathbf{A} and \mathbf{B} of the same size, we write $\mathbf{A} \leq \mathbf{B}$ to denote $a_{i,j} \leq b_{i,j}$ for all i, j ; and write $\mathbf{A} \circ \mathbf{B}$ to denote $(\mathbf{A} \circ \mathbf{B})_{i,j} = a_{i,j} b_{i,j}$. For $\mathbf{u} \in \mathbb{R}^n$, let $\underline{\mathbf{u}} := \mathbf{u} / \|\mathbf{u}\|_2$; the standard unit basis vectors are denoted $\mathbf{e}_i \in \mathbb{R}^n$, where the i^{th} entry is one and the others zero. We write diagonal matrices as $\mathbf{D}_{\mathbf{a}}$, where $(\mathbf{D}_{\mathbf{a}})_{i,i} = a_i$; we write the identity matrix as $\mathbf{I}_n \in \mathbb{R}^{n \times n}$. We define the τ -simplex $\mathbf{T} := \{\boldsymbol{\lambda} \in \mathbb{R}^p : \boldsymbol{\lambda}^\top \mathbf{1}_p = \tau, \boldsymbol{\lambda} \geq \mathbf{0}\}$, and the $\sqrt{\tau}$ -radius sphere surface manifold $\mathcal{S}_{\sqrt{\tau}} := \{\boldsymbol{\gamma} \in \mathbb{R}^p : \|\boldsymbol{\gamma}\|_2 = \sqrt{\tau}\}$. For consistency, we index samples with $i \in \{1, \dots, n\}$, quantiles with $j \in \{1, \dots, m\}$, covariates with $k \in \{1, \dots, p\}$, and constraints with $c \in \{1, \dots, m+1\}$. Finally, we denote a sequence of integers starting at one by $[n] := \{1, \dots, n\}$.

2 Data description

2.1 Data collection

The data used in this paper were collected as part of the hyperglycemic profiles in obstructive sleep apnea (HYPNOS) randomized clinical trial. The study population consisted of adults between 21 and 75 years old with type 2 diabetes recruited from the community. The primary objective of the trial was to determine whether treatment with positive airway pressure (PAP) therapy is associated with improvements in glycemic measures. Study participants were screened based on the point-of-care HbA1c measured with a DC Vantage Analyzer (Siemens, Malvern, PA) and a home sleep apnea test using the Apnealink monitor (Resmed, San Diego, CA). Participants with HbA1c $\geq 6.5\%$ and obstructive sleep apnea were invited to enroll in the study. Exclusion criteria included pregnancy, any prior therapy for OSA, use of insulin, change in glycemic medications in the previous 6 weeks, current oral steroid use, other sleep disorders, habitual sleep duration of < 6 h/night, and any unstable medical conditions. Study participants used Dexcom G4 Platinum CGM sensor, which produces one measurement every 5 min. The CGM was placed 6 cm lateral to the umbilicus. Participants were instructed to wear the monitor for at least 7 days and provide calibration glucose data for the sensor twice a day according to the manufacturer's instructions. To investigate the effects of OSA severity and other variables on the glucose control of patients with type 2 diabetes, we consider the data at the baseline visit (prior to the randomization of study participants into control and PAP therapy groups). The research protocol was approved by the Institutional Review Board on human research (Number: NA_00093188). A detailed description of the trial protocol and implementation can be found in [Rooney et al. \(2021\)](#).

2.2 Data processing

For each patient, we calculate an empirical quantile function of their CGM measurements corresponding to a baseline visit using a grid of $m = 100$ equally spaced points in $(0, 1)$, leading to response vector $\mathbf{y}_i \in \mathbb{R}^m$ corresponding to patient $i \in [n]$ with $n = 207$ patients. On average, there are 2871 glucose values for each patient, ranging from 742 to 5234 (given sensor's 5 min frequency, this corresponds to 2.6 days and 18.2

Demographic	Age	61	(28 - 75)
	Male Sex	113	54.3%
Diabetes-related	HbA1c	7.2%	(6.5% - 11.2%)
	Biguanide use	177	85.1%
	Sulfonylurea use	70	33.7%
OSA-related	ODI ₄	14.9	(2.0 - 128.6)
	Mean Saturation	92.7%	(74.2% - 96.8%)
	TST90%	8.4%	(0.2% - 98.9%)

Table 1: Selected descriptive statistics of the $n = 207$ patients used for analysis. Values are the medians (min-max) for continuous covariates or size (%) for binary covariates.

days, respectively). All but 10 subjects have ≥ 5 days of data. For each patient, we form a vector of baseline covariates $\mathbf{x}_i \in \mathbb{R}^p$ that contains demographic information (i.e., age, sex), clinical information (i.e., BMI, HbA1c), class of medications used, and variables related to OSA severity. We remove any medication that was used by four or fewer patients from the analysis, leading to $p = 34$ covariates total. Table 1 summarizes select characteristics of the study sample based on demographics, as well as covariates related to diabetes and OSA severity (Supplement S6 describes the full list of covariates). HbA1c values were obtained from point-of-care measurements taken before placement of the CGM sensor. Biguanides and sulfonylureas are families of oral drugs commonly prescribed for type 2 diabetes to reduce glucose levels. ODI₄ is the oxygen desaturation index corresponding to the rate of oxygen desaturation events of 4% or more, mean saturation is the overall average of the oxygen saturation during the recording period during sleep, and TST90% is the total sleep time with an oxygen saturation below 90% (represented as percentage).

2.3 Research questions and statistical challenges

Our primary scientific goal is to investigate the effects of measures of OSA and hyperglycemic medications on glucose distributions after accounting for other covariates. Fréchet regression with variable selection (Tucker et al., 2023) provides a methodological framework for selecting covariates that affect empirical quantile functions of glucose; however, the dimensions of HYPNOS data present computational challenges for the existing algorithm. Consequently, characterizing the uncertainty in variable selection within this framework is infeasible. Our methodological goals are to develop a fast algorithm for Fréchet regression with variable selection, and characterize variable selection uncertainty by evaluating the stability of selected covariates across subsamples (Meinshausen and Bühlmann, 2010).

3 Distributional regression via Fréchet regression

3.1 Fréchet regression

Petersen and Müller (2019) propose Fréchet regression by reformulating the conditional mean in linear regression to make underlying Euclidean geometry explicit. Given a random $Y \in \mathbb{R}$ and a realization \mathbf{x}_* of $X \in \mathbb{R}^p$, the conditional mean model in linear regression is $\mathbb{E}(Y|X = \mathbf{x}_*) = \beta_0 + \mathbf{x}_*^\top \boldsymbol{\beta}$, where $\boldsymbol{\beta} \in \mathbb{R}^p$ is a vector of coefficients. Consider an iid sample $\{(\mathbf{x}_i, y_i) \in \mathbb{R}^p \times \mathbb{R} : i \in [n]\}$, where $\mathbf{y} := (y_1 \dots y_n)^\top \in \mathbb{R}^n$, $\mathbf{X} := (\mathbf{x}_1 \dots \mathbf{x}_n)^\top \in \mathbb{R}^{n \times p}$ and we assume \mathbf{X} is column-centered. Petersen and Müller (2019) show that

least squares estimation from this sample leads to an estimator \hat{y}_* of the conditional mean which satisfies

$$\hat{y}_* := \arg \min_{y \in \mathbb{R}} \sum_{i=1}^n s_i(\mathbf{x}_*) \cdot (y - y_i)^2, \quad s_i(\mathbf{x}_*) = \frac{1}{n} + \mathbf{x}_*^\top (\mathbf{X}^\top \mathbf{X})^{-1} \mathbf{x}_i. \quad (1)$$

Petersen and Müller (2019) propose to replace the Euclidean space (\mathbb{R}, d_E^2) in (1)—that is, response $y \in \mathbb{R}$ with distance $d_E^2(y, y_i) = (y - y_i)^2$ —with a general metric space (Ω, d^2) , leading to the Fréchet regression

$$\hat{y}_* := \arg \min_{y \in \Omega} \sum_{i=1}^n s_i(\mathbf{x}_*) \cdot d^2(y, y_i), \quad s_i(\mathbf{x}_*) = \frac{1}{n} + \mathbf{x}_*^\top (\mathbf{X}^\top \mathbf{X})^{-1} \mathbf{x}_i. \quad (2)$$

We consider the case of Fréchet regression where Ω is the space of univariate quantile functions $\mathbf{Q} = \{\mathbf{q} : [0, 1] \mapsto \mathbb{R}\}$, equipped with the 2-Wasserstein distance d_W^2 , leading to

$$\hat{\mathbf{q}}_* = \arg \min_{\mathbf{q} \in \mathbf{Q}} \sum_{i=1}^n s_i(\mathbf{x}_*) \cdot d_W^2(\mathbf{q}, \mathbf{y}_i), \quad d_W^2(\mathbf{q}, \mathbf{p}) = \int_0^1 \{\mathbf{q}(u) - \mathbf{p}(u)\}^2 du \quad \forall \mathbf{q}, \mathbf{p} \in \mathbf{Q}. \quad (3)$$

In practice, we consider responses that are empirical quantile functions evaluated on the same uniformly spaced m -sequence in $(0, 1)$, i.e. $\mathbf{Y} = (\mathbf{y}_1 \dots \mathbf{y}_n)^\top \in \mathbb{R}^{n \times m}$ and $y_{i,j} \leq y_{i,j'}$ for $j \leq j'$, leading to the formulation

$$\hat{\mathbf{q}}_* = \arg \min_{\mathbf{q} \in \mathbb{R}^m} \sum_{i=1}^n s_i(\mathbf{x}_*) \cdot \|\mathbf{q} - \mathbf{y}_i\|_2^2, \quad \text{subject to} \quad \mathbf{b} - \mathbf{A}^\top \mathbf{q} \leq \mathbf{0}. \quad (4)$$

The constraints $\mathbf{b} - \mathbf{A}^\top \mathbf{q} \leq \mathbf{0}$ enforce monotonicity of $\hat{\mathbf{q}}$, as well as adherence to specified distribution support via box constraints $b_L \leq q_j \leq b_U$. The latter is necessary in our context as Dexcom CGM only records values in a $[40, 400]$ mg/dL range.

It is often necessary to evaluate predicted quantile functions $\hat{\mathbf{q}}_*$ at multiple \mathbf{x}_* , e.g., evaluate predictions on the training data. Below we show these predictions can be evaluated concurrently in a quadratic optimization problem; the proof is in Supplement S2.

Theorem 3.1. *Let $\mathbf{X} \in \mathbb{R}^{n \times p}$ be a column-centered covariate matrix, let $\mathbf{X}_* \in \mathbb{R}^{d \times p}$ consist of d covariate vectors $\mathbf{x}_* \in \mathbb{R}^p$ centered the same as \mathbf{X} , and let $\mathbf{Y} \in \mathbb{R}^{n \times m}$ row-wise consist of n empirical quantile functions $\{\mathbf{y}_i\}$ evaluated on a shared, uniformly dispersed m -grid over $(0, 1)$. Then for each row \mathbf{x}_* in \mathbf{X}_* , the corresponding $\hat{\mathbf{q}}_*$ in (4) satisfies*

$$\hat{\mathbf{q}}_* = \arg \min_{\mathbf{q} \in \mathbb{R}^m} \frac{1}{2} \|\mathbf{q} - \hat{\mathbf{y}}_*\|_2^2, \quad \text{subject to} \quad \mathbf{b} - \mathbf{A}^\top \mathbf{q} \leq \mathbf{0},$$

where $\hat{\mathbf{y}}_*^\top = \{n^{-1} \mathbf{1}_n^\top + \mathbf{x}_*^\top (\mathbf{X}^\top \mathbf{X})^{-1} \mathbf{X}^\top\} \mathbf{Y}$. Furthermore, the matrix $\hat{\mathbf{Q}}_* \equiv \hat{\mathbf{Q}}(\mathbf{X}_*) \in \mathbb{R}^{d \times m}$, which row-wise consists of $\hat{\mathbf{q}}_*$'s, satisfies

$$\hat{\mathbf{Q}}_* = \arg \min_{\mathbf{Q} \in \mathbb{R}^{d \times n}} \frac{1}{2} \|\mathbf{Q} - \hat{\mathbf{Y}}_*\|_F^2, \quad \text{subject to} \quad \mathbf{B} - \mathbf{Q} \mathbf{A} \leq \mathbf{0}, \quad (5)$$

where the rows of \mathbf{B} are each \mathbf{b} , and $\hat{\mathbf{Y}}_* := \{n^{-1} \mathbf{1}_{d \times n} + \mathbf{X}_* (\mathbf{X}^\top \mathbf{X})^{-1} \mathbf{X}^\top\} \mathbf{Y}$.

3.2 Variable Selection in Fréchet Regression

Tucker et al. (2023) extend Fréchet regression (Petersen and Müller, 2019) to allow for variable selection. They introduce (what we call) an “allowance vector” $\boldsymbol{\lambda} \in \mathbf{T} := \{\boldsymbol{\lambda} \in \mathbb{R}^p : \boldsymbol{\lambda}^\top \mathbf{1}_p = \tau, \boldsymbol{\lambda} \geq \mathbf{0}\}$ whose non-negative entries add to “total allowance” $\tau > 0$, with zero entries corresponding to eliminated variables. Tucker et al. (2023) replace $\hat{\mathbf{Y}}$ in Proposition 3.1 with $\hat{\mathbf{Y}}(\boldsymbol{\lambda}) = n^{-1}\{\mathbf{1}_{n \times n} + \mathbf{X}(n^{-1}\mathbf{X}^\top \mathbf{X} + \mathbf{D}_{\boldsymbol{\lambda}^{-1}})^{-1}\mathbf{X}^\top\}\mathbf{Y}$, which involves a generalized ridge penalty. This is an idea based on Wu (2021), who shows that generalized ridge regression can perform variable selection via tuning parameters inverse-proportional to elements of $\boldsymbol{\lambda}$. To prevent division by zero, $\hat{\mathbf{Y}}(\boldsymbol{\lambda})$ can be rewritten

$$\hat{\mathbf{Y}}(\boldsymbol{\lambda}) = n^{-1}\mathbf{1}_{n \times n}\mathbf{Y} + \mathbf{Y} - (\tilde{\mathbf{X}}\mathbf{D}_{\boldsymbol{\lambda}}\tilde{\mathbf{X}}^\top + \mathbf{I}_n)^{-1}\mathbf{Y}, \quad (6)$$

and the best $\hat{\boldsymbol{\lambda}}(\tau)$ is found as

$$\hat{\boldsymbol{\lambda}}(\tau) := \arg \min_{\boldsymbol{\lambda} \in \mathbf{T}} \frac{1}{2} \|\hat{\mathbf{Q}}(\boldsymbol{\lambda}) - \mathbf{Y}\|_F^2, \quad (7)$$

$$\hat{\mathbf{Q}}(\boldsymbol{\lambda}) := \arg \min_{\mathbf{Q} \in \mathbb{R}^{n \times m}} \frac{1}{2} \|\mathbf{Q} - \hat{\mathbf{Y}}(\boldsymbol{\lambda})\|_F^2, \quad \text{subject to } \mathbf{B} - \mathbf{Q}\mathbf{A} \leq \mathbf{0}. \quad (8)$$

We refer to (8) as the embedded problem and to (7) as the sparsity problem. A collection of solution paths $\{\hat{\boldsymbol{\lambda}}_k(\tau) : \tau \in (0, \tau_{\max}]\}_{k=1}^p$ can be obtained by varying τ over a user-specified range.

3.3 Review of existing algorithms

The existing algorithm to solve the embedded problem (8) is the `quadprog::solve.QP` R function (Turlach et al., 2019), a wrapper for a Fortran implementation of the dual-active set method of Goldfarb and Idnani (1983) for convex quadratic programming problems. However, the algorithm can only be applied to a single vector $\hat{\mathbf{q}}_i$ at a time, requiring an outer loop structure which slows the computations.

The existing algorithm to solve the sparsity problem (7) is a modified coordinate descent algorithm implemented in R language. The complete algorithm is described in Supplement S5. A single t^{th} iteration comprises a sequential loop through all coordinates $k \in [p]$. Inside the loop, the current $\boldsymbol{\lambda}^{(t)}$ is moved along the simplex-spanning line segment connecting it to the k^{th} corner of the simplex \mathbf{T} . The optimal step size is determined using `stats::optimize` function in R, which implements a golden-section line search method. The latter only requires evaluating the objective function value of (7) at a given $\boldsymbol{\lambda}$, making the algorithm sufficiently flexible for Fréchet regression on general metric spaces (Ω, d^2) . However, the overall algorithm is very slow, as only one coordinate of $\boldsymbol{\lambda}$ is updated at a time, and the update does not take advantage of the gradient of the objective function.

4 Proposed method

In this section, we develop a new fast algorithm for (7). First, we develop a dedicated algorithm for the embedded problem (8) that allows us to avoid matrix multiplications (Section 4.1). Second, we derive the gradient and Hessian of the objective function for the sparsity problem (Section 4.2). Finally, we utilize the gradient information to develop an unconstrained geodesic descent algorithm (Section 4.3).

4.1 Dedicated solver for embedded problem

In this section, we outline our proposed algorithm for solving the embedded problem (8). Specifically, we propose to perform projected gradient ascent on the Lagrange multipliers for the associated dual problem. The advantage of this approach is that it allows us to directly solve for the whole matrix $\mathbf{Q} \in \mathbb{R}^{n \times m}$ (rather than work with one $\mathbf{q}_i \in \mathbb{R}^m$ at a time), and take advantage of the special structure of matrix \mathbf{A} in constraints to make efficient matrix multiplications.

Let $\hat{\mathbf{Y}} = \hat{\mathbf{Y}}(\boldsymbol{\lambda})$, and consider $\mathcal{L}(\mathbf{Q}, \mathbf{H}) = \frac{1}{2} \|\mathbf{Q} - \hat{\mathbf{Y}}\|_F^2 + \text{tr} \{(\mathbf{B} - \mathbf{Q}\mathbf{A})\mathbf{H}^\top\}$, the Lagrangian for (8), where $\mathbf{H} \geq \mathbf{0}_{n \times (m+1)}$ is the matrix of associated Lagrange multipliers. Given the step size $\alpha > 0$, the update has the form $\mathbf{H}^{(t+1)} = \{\mathbf{H}^{(t)} + \alpha \nabla h(\mathbf{H}^{(t)})\}_+$, where $\nabla h(\mathbf{H}^{(t)})$ is the gradient of the dual function $h(\mathbf{H}) = \inf_{\mathbf{Q}} \mathcal{L}(\mathbf{Q}, \mathbf{H})$ evaluated at $\mathbf{H}^{(t)}$. By taking the gradients of the Lagrangian, we derive a closed-form update

$$\mathbf{H}^{(t+1)} = \left[\alpha \{ \mathbf{H}^{(t)} (\alpha^{-1} \mathbf{I}_m - \mathbf{A}^\top \mathbf{A}) + (\mathbf{B} - \hat{\mathbf{Y}}\mathbf{A}) \} \right]_+,$$

with final $\mathbf{Q}^{(t+1)} = \hat{\mathbf{Y}} + \mathbf{H}^{(t+1)}\mathbf{A}^\top$. We use $\alpha = 1/2$ in our implementation; thus each update requires evaluation of the matrix product $\mathbf{H}^{(t)}(2\mathbf{I}_m - \mathbf{A}^\top \mathbf{A})$. We show that this operation can be reduced to an addition operation by taking advantage of the specific structure of \mathbf{A} matrix. See Supplement S3 for full derivations.

4.2 Gradient and Hessian

In this section, we present the gradient and Hessian of the objective function in (7). We utilize the KKT conditions of the embedded optimizer $\hat{\mathbf{Q}}$ to derive the gradient, from which the Hessian easily follows. Derivations are in Supplement S2.

Theorem 4.1. *Let $\hat{\mathbf{Q}} = \hat{\mathbf{Q}}(\boldsymbol{\lambda})$ from (8). For each $i \in [n]$, let $\mathbf{A} = [\mathbf{A}_{0,i} \quad \mathbf{A}_{-,i}]$ be the block decomposition of \mathbf{A} into those columns corresponding to the active constraints on $\hat{\mathbf{q}}_i$ (i.e. $\mathbf{A}_{0,i}$) and those columns corresponding to inactive constraints (i.e. $\mathbf{A}_{-,i}$), with $\mathbb{P}_{\mathbf{A}_{0,i}}$ the orthogonal projector onto $\mathbf{A}_{0,i}$. If no constraints are active, let $\mathbb{P}_{\mathbf{A}_{0,i}} = \mathbf{0}$. Let $f(\boldsymbol{\lambda}) := \|\hat{\mathbf{Q}} - \mathbf{Y}\|_F^2/2$ be the objective function in (7), and let $\mathbf{G} := (\tilde{\mathbf{X}}\mathbf{D}_\lambda\tilde{\mathbf{X}}^\top + \mathbf{I}_n)^{-1}$ with $\tilde{\mathbf{X}} = \mathbf{X}/\sqrt{n}$. Then the gradient and Hessian of $f(\boldsymbol{\lambda})$ are respectively*

$$\nabla f(\boldsymbol{\lambda}) = \text{diag}(\mathbf{N}), \text{ where } \mathbf{N} := \tilde{\mathbf{X}}^\top \mathbf{G} \left\{ \sum_{i=1}^n \mathbf{e}_i \mathbf{e}_i^\top (\hat{\mathbf{Y}} - \mathbf{Y})(\mathbf{I}_m - \mathbb{P}_{\mathbf{A}_{0,i}}) \right\} \mathbf{Y}^\top \mathbf{G} \tilde{\mathbf{X}}; \quad (9)$$

$$\begin{aligned} \nabla^2 f(\boldsymbol{\lambda}) = & (\tilde{\mathbf{X}}^\top \mathbf{G} \mathbf{Y} \mathbf{Y}^\top \mathbf{G} \tilde{\mathbf{X}}) \circ (\tilde{\mathbf{X}}^\top \mathbf{G}^2 \tilde{\mathbf{X}}) - (\tilde{\mathbf{X}}^\top \mathbf{G} \tilde{\mathbf{X}}) \circ (\mathbf{N} + \mathbf{N}^\top) - \\ & \sum_{i=1}^n (\tilde{\mathbf{X}}^\top \mathbf{G} \mathbf{Y} \mathbb{P}_{\mathbf{A}_{0,i}} \mathbf{Y}^\top \mathbf{G} \tilde{\mathbf{X}}) \circ (\tilde{\mathbf{X}}^\top \mathbf{G} \mathbf{e}_i \mathbf{e}_i^\top \mathbf{G} \tilde{\mathbf{X}}). \end{aligned} \quad (10)$$

4.3 Geodesic descent algorithm

We propose to utilize the obtained gradient and Hessian (Proposition 4.1) in creating a faster algorithm for solving sparsity problem (7). Specifically, we develop a second-order geodesic descent algorithm by (i) changing the constraint set in (7) from simplex to sphere via a change of variables (Section 4.3.1); (ii) deriving constraint-preserving rotation steps along geodesics on the sphere via rotations (Section 4.3.2); (iii) choosing the optimal rotation angle at each step using the local Hessian of the reparameterized function (Section 4.3.3).

4.3.1 Simplex to spherical constraint

We propose to reparameterize the simplex constraints in (7) into spherical constraints, allowing unconstrained updates (Section 4.3.2). Let $\mathcal{F} : \mathcal{S}_{\sqrt{\tau}} \mapsto \mathbf{T}$ map the $\sqrt{\tau}$ -radius sphere to the simplex by $\mathcal{F}(\boldsymbol{\gamma}) = \boldsymbol{\gamma} \circ \boldsymbol{\gamma}$. Then for $\boldsymbol{\lambda} \in \mathbf{T}$, $\mathcal{F}^{\leftarrow}(\boldsymbol{\lambda}) = \{\boldsymbol{\gamma} \in \mathcal{S}_{\sqrt{\tau}} : \boldsymbol{\gamma} \circ \boldsymbol{\gamma} = \boldsymbol{\lambda}\}$ defines an equivalence class in $\mathcal{S}_{\sqrt{\tau}}$ leading to reparameterized sparsity problem (7) in terms of $\boldsymbol{\gamma}$

$$\hat{\boldsymbol{\lambda}} = \arg \min_{\boldsymbol{\lambda} \in \mathbf{T}} f(\boldsymbol{\lambda}) \quad \rightarrow \quad \hat{\boldsymbol{\gamma}} = \arg \min_{\boldsymbol{\gamma} \in \mathcal{S}_{\sqrt{\tau}}} (f \circ \mathcal{F})(\boldsymbol{\gamma}), \quad \hat{\boldsymbol{\gamma}} \in \mathcal{F}^{\leftarrow}(\hat{\boldsymbol{\lambda}}). \quad (11)$$

We propose performing gradient descent on (11) instead of (7). We next derive the gradient and Hessian of the objective function with respect to $\boldsymbol{\gamma}$, $g(\boldsymbol{\gamma}) = (f \circ \mathcal{F})(\boldsymbol{\gamma})$, by taking advantage of Proposition 4.1 and the chain rule. The full derivations are in Supplement S2.

Theorem 4.2. *Let $\boldsymbol{\lambda} = \mathcal{F}(\boldsymbol{\gamma}) = \boldsymbol{\gamma} \circ \boldsymbol{\gamma}$, and define composite function $g(\boldsymbol{\gamma}) := (f \circ \mathcal{F})(\boldsymbol{\gamma})$ as in (11). The gradient and Hessian of $g(\boldsymbol{\gamma})$ are respectively*

$$\nabla g(\boldsymbol{\gamma}) = 2\boldsymbol{\gamma} \circ (\nabla f \circ \mathcal{F})(\boldsymbol{\gamma}); \quad (12)$$

$$\nabla^2 g(\boldsymbol{\gamma}) = 2\mathbf{D}_{(\nabla f \circ \mathcal{F})(\boldsymbol{\gamma})} + 4(\boldsymbol{\gamma}\boldsymbol{\gamma}^\top) \circ (\nabla^2 f \circ \mathcal{F})(\boldsymbol{\gamma}), \quad (13)$$

where $(\nabla f \circ \mathcal{F})(\boldsymbol{\gamma}) \equiv \nabla f(\boldsymbol{\lambda})$ is from (9) and $(\nabla^2 f \circ \mathcal{F})(\boldsymbol{\gamma}) \equiv \nabla^2 f(\boldsymbol{\lambda})$ is (10).

4.3.2 Geodesic updates

Given the starting $\boldsymbol{\gamma}^{(0)} \in \mathcal{S}_{\sqrt{\tau}}$, we propose to utilize constraint-preserving optimization updates by conducting steps along geodesics in the sphere in the direction against the gradient. Specifically, the updates take the form

$$\boldsymbol{\gamma}^{(t+1)} = \mathbf{R}^{(t)} \boldsymbol{\gamma}^{(t)} \quad (14)$$

where rotations $\mathbf{R}^{(t)}$ on $\mathcal{S}_{\sqrt{\tau}}$ are geodesic steps, in contrast to linear steps in \mathbb{R}^p that may not be constraint-preserving. To rotate against the gradient, we decompose the gradient at the current $\boldsymbol{\gamma}^{(t)}$ as the sum of tangent and normal components to $\mathcal{S}_{\sqrt{\tau}}$ at $\boldsymbol{\gamma}^{(t)}$:

$$\nabla g(\boldsymbol{\gamma}^{(t)}) = (\mathbf{I}_p - \mathbb{P}_{\boldsymbol{\gamma}^{(t)}}) \nabla g(\boldsymbol{\gamma}^{(t)}) + \mathbb{P}_{\boldsymbol{\gamma}^{(t)}} \nabla g(\boldsymbol{\gamma}^{(t)}).$$

For brevity, we define

$$\mathbf{v}^{(t)} = -(\mathbf{I}_p - \mathbb{P}_{\boldsymbol{\gamma}^{(t)}}) \nabla g(\boldsymbol{\gamma}^{(t)}), \quad (15)$$

which is orthogonal to $\boldsymbol{\gamma}^{(t)}$. The rotation between orthonormal vectors $\underline{\boldsymbol{\gamma}}^{(t)} \rightarrow \underline{\mathbf{v}}^{(t)}$ by angle $\theta^{(t)}$ while fixing the orthogonal complement of $\text{span}(\boldsymbol{\gamma}^{(t)}, \mathbf{v}^{(t)})$ is

$$\boldsymbol{\gamma}^{(t+1)} = \mathbf{R}^{(t)} \boldsymbol{\gamma}^{(t)} = \cos(\theta^{(t)}) \boldsymbol{\gamma}^{(t)} + \sqrt{\tau} \sin(\theta^{(t)}) \underline{\mathbf{v}}^{(t)} \quad (16)$$

(proof is given in Supplement S1). By construction, $\boldsymbol{\gamma}^{(t+1)}$ is guaranteed to be feasible for (11). The remaining part in executing (16) is choosing a step size, that is, choosing the rotation angle $\theta^{(t)} > 0$.

4.3.3 Selecting the rotation angle

To choose the rotation angle $\theta^{(t)}$ in (16), we modify the optimized second-order Taylor expansion of $g(\boldsymbol{\gamma})$ around the circle. Specifically, we let

$$\theta^{(t)} = \min \left\{ \left| \frac{\frac{d}{d\theta} g_*^{(t)}(0)}{\frac{d^2}{d\theta^2} g_*^{(t)}(0)} \right|, \theta_{\max} \right\}, \quad (17)$$

where $\theta_{\max} = \pi/4$, and $g_*^{(t)}(\theta) := (g \circ \mathbf{R}^{(t)})(\boldsymbol{\gamma}^{(t)})$. Further, we derive the closed form of the first and second total derivatives of the composite function $g_*(\theta)$ with respect to θ , evaluated at $\theta = 0$. Derivations are given in Supplements S2; see also Supplement S4.

Theorem 4.3. *Let $\boldsymbol{\gamma} \in \mathcal{S}_{\sqrt{\tau}}$ and assume $\mathbf{v} \neq \mathbf{0}$. The first and second total derivatives of $g_*(\theta) := (g \circ \mathbf{R}_\theta)(\boldsymbol{\gamma})$, evaluated at $\theta = 0$, are respectively*

$$g'_*(0) = -\sqrt{\tau} \cdot \|\mathbf{v}\|_2, \quad (18)$$

$$g''_*(0) = \tau \cdot \underline{\mathbf{v}}^\top [\nabla^2 g(\boldsymbol{\gamma})] \underline{\mathbf{v}} - \boldsymbol{\gamma}^\top \nabla g(\boldsymbol{\gamma}). \quad (19)$$

4.3.4 Summary

In summary, we solve (7) by recasting the problem as (11). We use iterative rotations of $\boldsymbol{\gamma}^{(t)}$ via (16) with the angle $\theta^{(t)}$ set as in (17). We perform these rotations until a norm convergence condition $\|\boldsymbol{\gamma}^{(t+1)} - \boldsymbol{\gamma}^{(t)}\|_\infty \leq \varepsilon$ is met. We use $\hat{\boldsymbol{\gamma}}$ at convergence to set $\hat{\boldsymbol{\lambda}} = \hat{\boldsymbol{\gamma}} \circ \hat{\boldsymbol{\gamma}}$, and select variables based on corresponding nonzero elements of $\hat{\boldsymbol{\lambda}}$. We implemented our algorithm in C++ and made it available in R using Rcpp interface (Eddelbuettel and Francois, 2011). We use algebraically equivalent implementations to avoid large square matrices in e.g. the $p \gg n$ or $n \gg p$ cases; see Supplement S4 for details.

5 Stability selection

The selected model for (7) depends on τ . Tucker et al. (2023) propose K -fold cross-validation with refitting to select τ which minimizes out-of-sample error. This method has limitations: the results of cross-validation may be split-dependent; the final set of selected variables must correspond to one of the models on the solution path of (7), which may not contain the true model; and cross-validation for variable selection comes with no general theoretical guarantees. In sparse linear regression, stability selection is an alternative variable selection approach that overcomes these limitations of cross-validation (Meinshausen and Bühlmann, 2010). At a high level, stability selection consists of taking repeated subsamples of the full data, performing variable selection for each, and then measuring selection frequency across subsamples. The final model is determined by selecting variables with the highest selection frequency, with theoretical guarantees provided on the number of false discoveries as a function of the selection threshold. Our new proposed geodesic descent algorithm for (7) is fast, in contrast to the original algorithm, making computationally demanding subsampling-based methods for variable selection feasible. We adopt the complementary pairs stability selection (Shah and Samworth, 2013), which leads to tighter error bounds compared to Meinshausen and Bühlmann (2010).

At each subsampling step $b \in [B]$, let $\mathcal{I}_b, \mathcal{I}_b^c \subset [n]$ be randomly drawn complementary index sets of size $\lfloor n/2 \rfloor$ (half of the samples) i.e. $\mathcal{I}_b \cap \mathcal{I}_b^c = \emptyset$. Let $(\mathbf{X}^{\mathcal{I}_b}, \mathbf{Y}^{\mathcal{I}_b})$ and $(\mathbf{X}^{\mathcal{I}_b^c}, \mathbf{Y}^{\mathcal{I}_b^c})$ denote the corresponding subsets

of the full (\mathbf{X}, \mathbf{Y}) . Given $\tau > 0$, the selected variables for each subset are determined based on non-zero elements of $\hat{\boldsymbol{\lambda}}$ from (7), that is

$$\hat{S}_b(\tau) := \{k : \hat{\lambda}_k(\tau; \mathbf{X}^{\mathcal{I}_b}, \mathbf{Y}^{\mathcal{I}_b}) > 0\}, \quad \hat{S}_b^c(\tau) := \{k : \hat{\lambda}_k(\tau; \mathbf{X}^{\mathcal{I}_b^c}, \mathbf{Y}^{\mathcal{I}_b^c}) > 0\}.$$

The stability measure of the k^{th} variable is defined as its empirical selection probability across all subsamples and complementary subsets

$$\hat{\Pi}_B(k; \tau) := \frac{1}{2B} \sum_{b=1}^B \left[\mathbb{1}\{k \in \hat{S}_b(\tau)\} + \mathbb{1}\{k \in \hat{S}_b^c(\tau)\} \right]. \quad (20)$$

Higher $\hat{\Pi}_B(k; \tau)$ means more frequent selection of the k^{th} variable, giving more evidence for its importance. A selected variable set is defined with only those variables that have high selection frequency, i.e. $\hat{S}(\tau) := \{k : \hat{\Pi}_B(k; \tau) \geq \pi_{\text{thr}}\}$ for some threshold $0 < \pi_{\text{thr}} \leq 1$. The value of π_{thr} can be chosen to control the variable selection error, as we describe below.

Shah and Samworth (2013) derive several bounds on variable selection error with complementary pairs stability selection, which rely on individual selection probabilities of the underlying base procedure (in our case, selection based on non-zero elements in $\hat{\boldsymbol{\lambda}}$ from (7)). The bounds control the expected number of variables in $\hat{S}(\tau)$ that have low selection probability under the base procedure without making any assumptions on the base procedure itself. These bound can be interpreted in terms of falsely selected variables under additional assumptions that the base procedure is no worse than random guessing, and that the selection of noise variables is exchangeable. Here we adopt the tightest bound, which is obtained under mild shape restrictions on the distribution of the proportion of times a variable is selected (r -concavity, we refer to Shah and Samworth (2013) for details).

Theorem 5.1 (Bound (8) from Shah and Samworth (2013)). *Let $\phi \in (0, 1)$, and let $L_\phi \subset [p]$ be the set of variables with low selection probability (below ϕ) under base procedure (7). Let $\hat{S}(\tau)$ be the set of variables selected with complementary pairs stability selection using B subsamples and threshold π_{thr} . Then, under the assumption of r -concavity,*

$$E_L(\tau) = \mathbb{E}|\hat{S}(\tau) \cap L_\phi| \leq d(B, \pi_{\text{thr}}, \phi)|L_\phi|. \quad (21)$$

In (21), $d(B, \pi_{\text{thr}}, \phi)$ is a known function that depends on B , π_{thr} and ϕ ; and $|L_\phi|$ is the cardinality of L_ϕ . Shah and Samworth (2013) recommend choosing $B = 50$ to satisfy assumption of r -concavity, and setting $\phi = q/p$, where $q \equiv q(\tau)$ is the expected model size from (7) with a given τ and sample size $\lfloor n/2 \rfloor$. The latter choice implies that the variables with low selection probability have a selection frequency at most as high as random guessing, which makes them noise variables when the base procedure is no worse than random guessing. Since the number of noise variables is unknown, in practice bound (21) is applied with $|L_\phi|$ replaced by p . To estimate q , we sum $\hat{\Pi}_B(k; \tau)$ across all variables k . Finally, the value of $\pi_{\text{thr}}(\tau)$ is selected to control the bound at a fixed level, i.e., such that $E_L(\tau) \leq K$ for a given K . The higher is $\pi_{\text{thr}}(\tau)$, the lower is the bound.

In simulations (Section 6.2), we evaluate how tight is the bound using $K = 1$ and $K = 2$. Since $\hat{\Pi}_B(k; \tau)$ —and consequently, q and selected π_{thr} —depend on τ , we consider how $\hat{\Pi}_B(k; \tau)$ change across a range of τ values (stability paths), and choose those variables whose stability paths exceed $\pi_{\text{thr}}(\tau)$ at least once over the path. Since large values of τ in (7) lead to all variables being selected, in practice we restrict

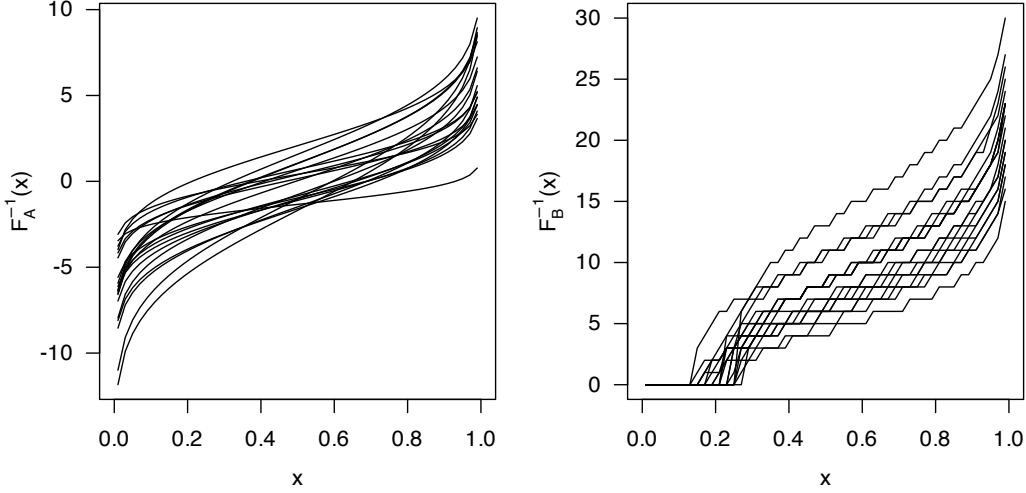


Figure 2: Example empirical quantile functions from Experiment A (*left*) and Experiment B (*right*) using $m = 50$ discretization.

the range of τ values so that the selected model size is at most $2/3$ of the total variables, that is $q(\tau)/p \leq 2/3$.

6 Simulation Studies

6.1 Algorithmic performance

In this section, we evaluate the performance of our proposed geodesic second-order descent (GSD) algorithm and compare it to existing modified coordinate descent (MCD) algorithm of [Tucker et al. \(2023\)](#). For MCD, we use the default implementation in R provided as supplement to [Tucker et al. \(2023\)](#). For GSD, we use our implementation with $\varepsilon = 0.0075$ (Section 4.3.4), chosen to ensure comparable or favorable convergence accuracy against default MCD implementation. In each experiment, we evaluate the total wall clock time (in seconds), and objective function values of (7) at convergence. We consider two settings for synthetic data generation, which we refer to Experiments A and B, described below.

Experiment A. We replicate Example 5.2.2 from [Tucker et al. \(2023\)](#). The random quantile function is generated conditionally on $\mathbf{x} \in \mathbb{R}^p$ as $\mathbf{q}(\cdot) = \mu_{\mathbf{x}} + \sigma_{\mathbf{x}}\Phi^{-1}(\cdot)$, with $\mu_{\mathbf{x}} \sim \mathcal{N}(\mu_0 + \beta(x_2 + x_3), \nu_1)$ and $\sigma_{\mathbf{x}} \sim \text{Gamma}((\sigma_0 + \kappa x_1)^2/\nu_2, \nu_2/(\sigma_0 + \kappa x_1))$. Hyper-parameters are as used in [Tucker et al. \(2023\)](#). Only the first three covariates affect \mathbf{q} .

Experiment B. We consider a less favorable setting for GSD, where the constraints in (8) are more likely to be active, requiring more computationally demanding evaluations of $\mathbb{P}_{\mathbf{A}_{0,i}}$ for (4.2). We use the zero-inflated negative binomial distribution with pmf $p(z) = \alpha_{\mathbf{x}}\mathbb{1}\{z = 0\} + (1 - \alpha_{\mathbf{x}})p_{Z|\mathbf{x}}(z)$, where $Z|\mathbf{x} \sim \text{nbinom}(r_{\mathbf{x}}, \pi_{\mathbf{x}})$. The random quantile function is generated conditionally on $\mathbf{x} \in \mathbb{R}^p$ as $\mathbf{q}(\cdot) = F_{Z|\mathbf{x}}^{-1}\{(\cdot - \alpha_{\mathbf{x}})/(1 - \alpha_{\mathbf{x}})\}$. We set $\text{logit}(\alpha_{\mathbf{x}}) \sim \mathcal{N}(\mu_{\alpha} + \beta_{\alpha}x_4, \nu_{\alpha})$, $\text{logit}(\pi_{\mathbf{x}}) \sim \mathcal{N}(\mu_{\pi} + \beta_{\pi}x_3, \nu_{\pi})$, $\log(r_{\mathbf{x}}) \sim \mathcal{N}(\mu_r + \beta_r(x_1 + x_2), \nu_r)$. We set $\mu_{\alpha} = \text{logit}(0.2)$, $\beta_{\alpha} = 0.4$, and $\nu_{\alpha} = 0.1^2$; $\mu_{\pi} = \text{logit}(0.5)$, $\beta_{\pi} = 0.1$, and $\nu_{\pi} = 0.15^2$; and $\mu_r = \log(10)$, $\beta_r = 0.2$, and $\nu_r = 0.15^2$. Only the first four covariates affect \mathbf{q} .

Figure 2 illustrates 20 example discretized quantile functions from each experiment.

Run Times. Figure 3 compares wall clock times for MCD and GSD to solve the sparsity problem (7). For each combination of parameter settings $n \in \{12, 25, 50, 100, 200\}$, $p \in \{10, 20\}$, and $m \in \{25, 50\}$, we

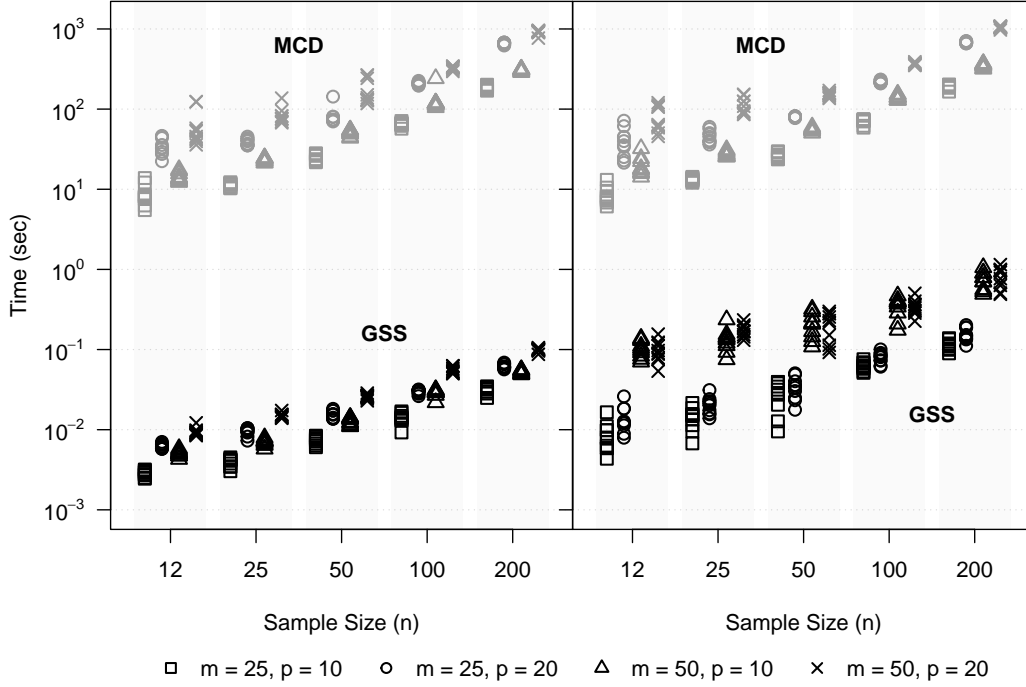


Figure 3: Sparsity algorithm wall clock times on $\tau \in [20]$, Experiment A (*left*) and Experiment B (*right*). MCD times in grey, GSD times in black.

generated ten data sets from Experiment A and Experiment B each. Solution paths $\lambda(\tau \in [20])$ were generated independently with MCD and GSD with initial allowance vector $\lambda^{(0)}(\tau = 20) = (\tau/p)\mathbf{1}_p$. Wall clock times were estimated for one replication each with R’s `microbenchmark` package (Mersmann, 2023) on a Mac OS system with Apple M1 Max chip. While our implementation of GSD has an advantage over MCD due to the underlying code being in C++ rather than R, the conclusions from timing comparisons still hold true with our earlier version of algorithm in R. As expected, the higher n , p , and m , the more difficult the problem. In Experiment B, larger m generally means more instances of active lower box constraints on \hat{Q} , lending to more frequent and expensive evaluations of $\mathbb{P}_{A_{0,i}}$ in (9). Such a problem does not occur for MCD, which does not evaluate the gradient. Despite this, the GSD algorithm is several orders of magnitude faster, and has more favorable scaling with n and p than MCD.

Accuracy. Figure 4 compares optimization accuracy between MCD and GSD across $\tau \in [20]$, fixing $n = 50$, $p = 10$, and $m = 50$. Within each experiment setting, the two algorithms were pairwise compared using 21 replications. For each replication, we plot $\log_{10} \frac{f(\lambda_{\text{MCD}}^{(t)})}{f(\lambda_{\text{GSD}}^{(t)})}$ against τ , so that positive values indicate GSD out-performing MCD. The two algorithms have comparable accuracy in both simulation settings.

6.2 Variable selection performance

In this section, we compare the variable selection performance of 10-fold cross-validation against complementary pairs stability selection as described in Section 5. We consider Experiment A with $n \in \{50, 100, 200\}$, $p \in \{10, 30\}$, and $m = 50$, with 100 replicates for each setting. We use a fine grid $\tau_{\text{CV}} \in \{10, 9.9, \dots, 0.1\}$ for cross-validation; and coarse grid $\tau_{\text{SS}} \in \{10, 9.5, \dots, 0.5\}$ for stability selection. To avoid edge cases with stability selection (all variables being selected with sufficiently large τ), we only consider stability paths over

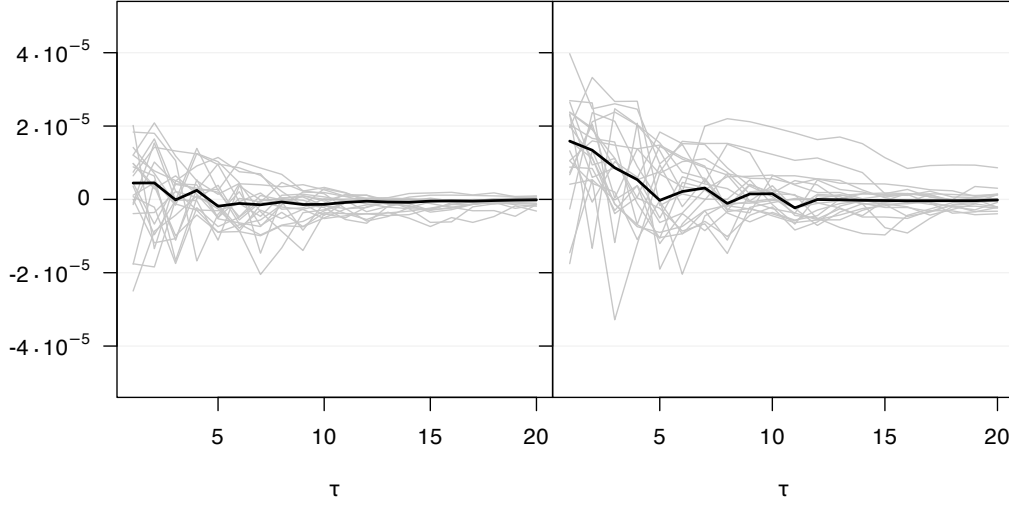


Figure 4: Sparsity algorithm optimization accuracy comparison on 21 synthetic data sets from Experiment A (*left*) and Experiment B (*right*). Gray lines are $\log_{10}\{f(\boldsymbol{\lambda}_{\text{MCD}}^{(t)})/f(\boldsymbol{\lambda}_{\text{GSD}}^{(t)})\}$, evaluated on $\tau \in \{1, \dots, 20\}$ for each data set; the median values per τ across the respective 21 data sets are given by thick black lines.

		$\hat{P}[\text{true selection}]$			$\hat{\mathbb{E}}[\text{false selections}]$		
		$\text{CV}_{K=10}$	$\text{SS}_{E \leq 1}$	$\text{SS}_{E \leq 2}$	$\text{CV}_{K=10}$	$\text{SS}_{E \leq 1}$	$\text{SS}_{E \leq 2}$
$p = 10$	$n = 50$	0.83	0.75	0.82	0.92	0.09	0.17
	$n = 100$	0.98	0.98	0.98	0.49	0.08	0.13
	$n = 200$	1.00	1.00	1.00	0.30	0.07	0.09
$p = 30$	$n = 50$	0.78	0.74	0.82	1.34	0.35	0.91
	$n = 100$	0.93	0.96	0.98	0.45	0.37	0.83
	$n = 200$	1.00	1.00	1.00	0.24	0.35	0.82

Table 2: Variable selection performance comparison between 10-fold cross validation ($\text{CV}_{K=10}$), and complementary pairs stability selection with bound (21) controlled at $\{1, 2\}$ ($\text{SS}_{E \leq 1}$, $\text{SS}_{E \leq 2}$). $\hat{P}[\text{true selection}]$ is estimated power (probability of true variable being selected), and $\hat{\mathbb{E}}[\text{false selections}]$ is the average number of falsely selected variables. All results are averaged over 100 replications of Experiment A.

the range of τ that lead to model size at most $2/3$ of the total p , that is $q(\tau)/p \leq 2/3$. For stability selection, we calculate minimal $\pi_{\text{thr}}(\tau_{\text{SS}})$ for each τ_{SS} to control (21) as $E_L(\tau_{\text{SS}}) \leq 1$ and $E_L(\tau_{\text{SS}}) \leq 2$, respectively.

We evaluate $\hat{P}[\text{true selection}]$, the average proportion of the true variable being selected (power, averaged across the first three true variables), and $\hat{\mathbb{E}}[\text{false selections}]$, average number of falsely selected variables. Table 2 summarizes the results for each method. Stability selection provides comparable or improved power compared to cross-validation, while false discovery comparison depends on p . As expected, the increase in bound for stability selection from $E_L(\tau) \leq 1$ to $E_L(\tau) \leq 2$ increases power when $n = 50$. The number of actual false discoveries is well-within the bound in both cases, confirming the observation in Shah and Samworth (2013) that the bound is conservative and not tight, especially when p is relatively small; even with the more lenient $E_L(\tau) \leq 2$ bound, stability selection has vlow number of expected false discoveries (< 1).

7 Analysis of HYPNOS data

In this section, we utilize Fréchet regression to analyze the HYPNOS data described in Section 2. We apply the proposed geodesic descent algorithm to solve (7), and combine it with complementary pairs stability selection described in Section 5 to perform variable selection inference. The entire data have empirical quantile functions of $n = 207$ patients stored at $m = 100$ quantile discretization, with $p = 34$ covariates for each patient. As Dexcom G4 CGM measures glucose values in $[40, 400]$ mg/dL range, the embedded problem (8) is solved with box constraints (in addition to monotonicity constraints). The overarching goal of the analysis is to elucidate which patients’ characteristics affect their glucose distribution and quantify in which way, with a specific focus on the effect of potentially modifiable factors (medications and measures of OSA severity).

Covariate correlation for variables related to oxygen saturation: Before applying stability selection, we calculate pairwise correlations across all $p = 34$ covariates. High correlations (positive or negative) may present issues for stability selection as has been demonstrated by [Faletto and Bien \(2022\)](#) in the context of sparse linear regression with LASSO. In the presence of high correlations, variable selection becomes unstable, with stability selection “splitting the vote” across the variables in the correlated group, leading to low individual stability measures and, consequently, missed selections of true variables. In the HYPNOS data, we found that most covariates have low correlations, except for the five variables associated with measurements of oxygen saturation overnight, which form a correlated cluster: (1) ODI₄, (2) mean saturation, (3) minimum saturation, (4) standard deviation of oxygen saturation, and (5) TST90%. To circumvent the correlation issue, we perform principal component analysis on these five variables, and use the extracted principal components as covariates instead of original variables, still leading to $p = 34$. Supplement S6 provides additional details.

Computation time: We calculated stability measures (20) for each covariate using $B = 50$ complementary pairs on each of $\tau \in \{0.5, 1, \dots, 20\}$ leading to a total of 2000 evaluations of (11). Computationally, using convergence tolerance $\varepsilon = 10^{-5}$ (Section 4.3.4), this analysis took 4 minutes total using the proposed geodesic descent algorithm. Based on comparisons in simulations (Figure 3), such analysis would not be feasible with the original algorithm of [Tucker et al. \(2023\)](#).

Stability selection results: Figure 5 displays stability paths for each covariate, with the $\pi_{\text{thr}}(\tau)$ path guaranteeing $E_L(\tau) \leq 2$ (see Section 5). We used this bound based on simulation results in Section 6, to maximize power while maintaining acceptable error bounds. For comparison, we also include estimated relative model size $\hat{q}(\tau)/p$, which peaks just below $2/3$ at $\tau = 20$. The final selected variable set includes three covariates: HbA1c, sulfonylurea medication, and the 2nd principal component for oxygen saturation variables (PC_{2,oxygen}). The solution paths of three other covariates come within 0.1 of the $\pi_{\text{thr}}(\tau)$ path, all indicators for use of a medication: non-steroidal anti-inflammatory drug (NSAID), H1 antagonist, and angiotensin-II receptor blocker (A2RB).

Effects interpretation: To elucidate how the selected variables affect the distribution of glucose values, we obtain a refitted model using (4) with the selected three covariates. To investigate the sensitivity of inference to this selection, Supplement S6 provides the same analysis using the larger subset with NSAID, H1 antagonist, and A2RB indicators included; the interpretations of top three variables remain the same. Figure 6 illustrates predicted densities obtained by individually varying each of the three covariates, while keeping the remaining two covariates at fixed levels (HbA1c = 7.5%; sulfonylurea selected as “no”, median value; PC_{2,oxygen} = 0).

For HbA1c, higher values correspond to higher glucose readings ($126.2 \rightarrow 236.7$ mg/dL mean change

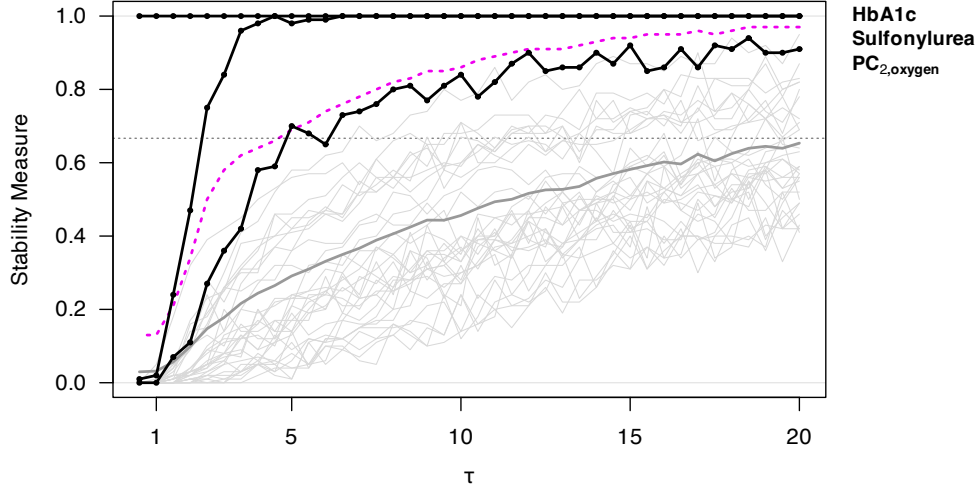


Figure 5: HYPNOS data set stability paths (20) from $B = 50$ complementary pairs subsets at each $\tau \in \{0.5, 1, \dots, 20\}$. Highlighted are the stability threshold $\pi_{\text{thr}}(\tau)$ guaranteeing $E_L(\tau) \leq 2$ (bold magenta line); variables selected by the “any vote” method (bold black lines), i.e. paths which exceed $\pi_{\text{thr}}(\tau)$ for some τ ; and average relative model size $\hat{q}(\tau)/p$ (bold gray line). A horizontal dotted line at $2/3$ is plotted for reference.

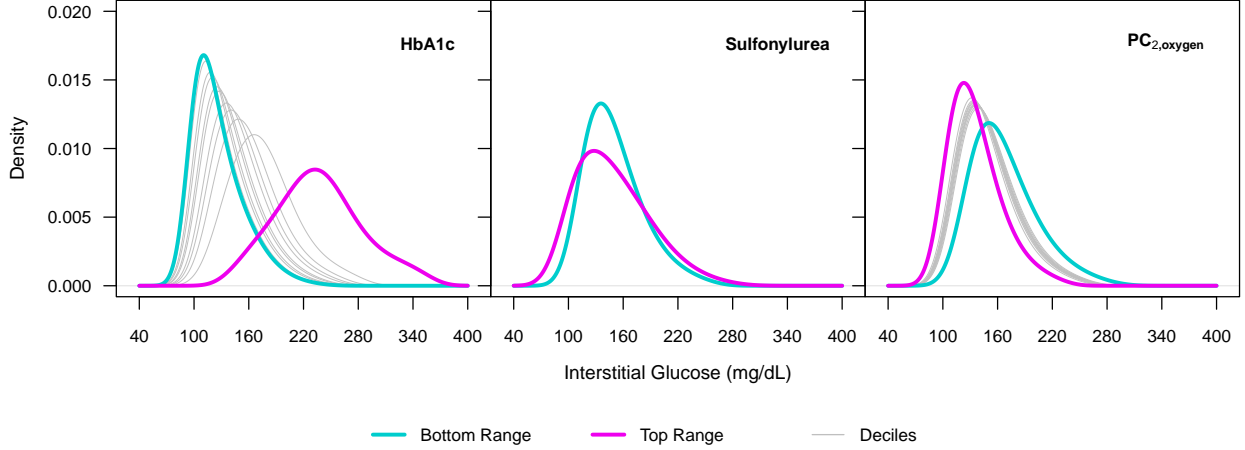


Figure 6: Predicted densities using Fréchet regression with 3 selected variables. In each panel, the levels of the corresponding covariate are varied from the lowest/“no” (bottom range, cyan) to the highest/“yes” (top range, magenta). Grey lines correspond to evaluations at 0.1 decile changes in corresponding variable. The remaining variables are kept constant, at sample mean for HbA1c, “no” for sulfonylurea use, and zero for $\text{PC}_{2,\text{oxygen}}$.

across the observed HbA1c range, i.e. from 6.5% to 11.2%). This is an expected result, as HbA1c corresponds to the average glucose over the preceding 2-3 months. While this HbA1c measurement was obtained before CGM placement, there is a significant correlation in average glucose values in subsequent months in the absence of interventions (Huang et al., 2021), and thus the association with mean CGM values in the preceding two weeks is expected. We found that higher HbA1c values were also predictive of higher variability ($28.9 \rightarrow 49.2$ mg/dL SD change across the observed range).

For sulfonylurea, we find that the use of medication is associated with an increase in glucose variability

(33.2 \rightarrow 42.1 mg/dL *SD* change), but no mean change (< 1 mg/dL). This is an unexpected result since sulfonylurea is a glucose-lowering medication that promotes insulin release from the pancreatic beta-cell; thus, we anticipated a lower mean value with medication use. However, in performing a literature search, we found that the same result was obtained when analyzing longitudinal HbA1c values of patients with type 2 diabetes in the ACCORD trial (German et al., 2022). Since neither HYPNOS nor ACCORD trials were designed to evaluate the effect of sulfonylurea, a possible explanation is that the patients who were prescribed sulfonylurea had higher glucose mean values at baseline than the patients who were not, and that resulting increased insulin secretion led to lowering of the mean (matching the one of patients not on medication) while at the same time increasing variability (more common lower values due to insulin). Further studies would be required to validate this conclusion.

For $PC_{2,\text{oxygen}}$, we found that high values are associated with lower glucose levels (167.3 \rightarrow 135.5 = -31.8 mg/dL mean change across the observed $PC_{2,\text{oxygen}}$ range) with a decrease in variability (37.1 \rightarrow 29.9 mg/dL *SD* change). To interpret this result in the context of original covariates, we consider the loadings associated with $PC_{2,\text{oxygen}}$, and create pairwise scatterplots of all five oxygen covariates, coloring the patients by low and high $PC_{2,\text{oxygen}}$ values (see Table S1 and Figure S3 in Supplement S6). We observe that low values of $PC_{2,\text{oxygen}}$ correspond to unstable oxygen saturation levels overnight, that is higher standard deviation of oxygen saturation overnight, coupled with more frequent or deep oxygen desaturation events. In contrast, patients with high values of $PC_{2,\text{oxygen}}$ (lower predicted glucose levels) tend to have lower overall saturation values and significantly lower saturation level variability overnight. Surprisingly, the $PC_{1,\text{oxygen}}$ covariate, which is reflective of the overall oxygen desaturation levels, isn't close to the top variable set (rank 25-34 of 34 across τ ; $\max_{\tau} \hat{\Pi}(k; \tau) = 0.46$).

8 Discussion

In this work, we develop a new algorithm for fast distributional regression that is fast and accurate, making methodology computationally feasible on large datasets and enabling the use of subsampling-based methods (stability selection) for variable selection inference. We demonstrate the effectiveness of our approach on both synthetic data and in application to CGM data from the HYPNOS study. We anticipate that our method opens the door to applying sparse distributional regression to other large-scale datasets.

In the analysis of CGM data from the HYPNOS study, we identified a few important covariates. While the selection of HbA1c, a measure of pre-study glucose levels, is not surprising, we found that sulfonylurea usage is associated with higher glucose variability without evidence of association with glucose mean, an association that regression methods on glucose summary statistics might fail to identify. Since the HYPNOS trial was not designed to evaluate the effect of sulfonylurea, further studies would be of interest to validate this association. We also found that overnight oxygen desaturation variability, as captured by the 2nd principal component associated with oxygen saturation covariates, has a stronger association with glucose distributions than the overall oxygen desaturation levels, as captured by the 1st component. To the best of our knowledge, this result is new and also unexpected in light of the common practice of only using ODI_4 covariate (measuring the rate of oxygen desaturation events) to characterize OSA severity, including prior analyses on HYPNOS data (Aurora et al., 2022; Sergazinov et al., 2023). Our findings suggest that the "stability" of saturation profiles overnight plays a crucial role in glucose regulation and that this "stability" is not fully captured by ODI_4 on its own. Subsequently, in future research, it would be of interest to better define the clinical implications of this association and validate it via replications in other studies. Finally,

our analyses revealed potential associations between glycemic control and three other medication types (non-steroidal anti-inflammatory drug, H1 antagonist, and angiotensin-II receptor blocker), albeit their selection frequencies were slightly smaller than the stability selection threshold. These medications are prescribed for conditions other than diabetes and are thus not typically considered as part of the diabetes management plan. Our literature search indicated that prior research in animal models also indicated associations between these medications and glycemic control (Anvari et al., 2015; Chu et al., 2006; Mortazavi-Jahromi et al., 2019), providing potential corroboration for our results and warranting follow-up validation studies.

From the methodological perspective, the scalability of our method is primarily achieved due to newly obtained closed-form expressions of gradient and Hessian associated with the sparse distributional regression problem. As indicated by Tucker et al. (2023), characterization of the gradient is required for theoretical analysis of convergence guarantees of the selection operator (7), and we hope our work opens the door for such further analysis. Furthermore, while we pursued geodesic descent algorithm, other optimization methods can take advantage of closed-form gradient expressions, such as conditional gradient family methods (Braun et al., 2022). Finally, in developing our method, we discovered that the idea of replacing the simplex constraint with a spherical constraint has also been explored by Li et al. (2023) in other optimization settings, who also provide theoretical convergence guarantees when objective function is convex.

Direct application of this result to our case is not possible as objective function $f(\lambda)$ in (7) can fail to be convex due to possibility of negative eigenvalues in Hessian in (10). While in practice our algorithm has always converged, a formal convergence analysis of the proposed algorithm and complete characterization of the stationary points of $f(\lambda)$ remain open problems for future research.

Funding

This work was supported by the NSF DMS-2044823.

Supplementary materials

Detailed derivations, propositions proofs, and additional simulation and real data analysis results.

References

- Ahmad, F. B., Cisewski, J. A., Xu, J. and Anderson, R. N. (2023), ‘Provisional mortality data — united states, 2022’, *MMWR. Morbidity and Mortality Weekly Report* **72**(18), 488–492.
- Anvari, E., Wang, X., Sandler, S. and Welsh, N. (2015), ‘The h1-receptor antagonist cetirizine ameliorates high-fat diet-induced glucose intolerance in male c57bl/6 mice, but not diabetes outcome in female non-obese diabetic (nod) mice’, *Upsala Journal of Medical Sciences* **120**(1), 40–46.
- Aurora, R. N., Gaynanova, I., Patel, P. and Punjabi, N. M. (2022), ‘Glucose profiles in obstructive sleep apnea and type 2 diabetes mellitus’, *Sleep Medicine* **95**, 105–111.
- Battelino, T., Alexander, C. M., Amiel, S. A., Arreaza-Rubin, G., Beck, R. W., Bergenstal, R. M., Buckingham, B. A., Carroll, J., Ceriello, A., Chow, E., Choudhary, P., Close, K., Danne, T., Dutta, S., Gabbay, R., Garg, S., Heverly, J., Hirsch, I. B., Kader, T., Kenney, J., Kovatchev, B., Laffel, L., Maahs, D., Mathieu, C., Mauricio, D., Nimri, R., Nishimura, R., Scharf, M., Del Prato, S., Renard, E., Rosenstock, J., Saboo, B., Ueki, K., Umpierrez, G. E., Weinzimer, S. A. and Phillip, M. (2022), ‘Continuous glucose

- monitoring and metrics for clinical trials: An international consensus statement', *The Lancet Diabetes & Endocrinology* p. S2213858722003199.
- Braun, G., Carderera, A., Combettes, C. W., Hassani, H., Karbasi, A., Mokhtari, A. and Pokutta, S. (2022), 'Conditional gradient methods'. preprint, arXiv:2211.14103 [math.OC].
- Callaghan, T., Ferdinand, A. O., Akinlotan, M. A., Towne, Jr, S. D. and Bolin, J. (2020), 'The changing landscape of diabetes mortality in the united states across region and rurality, 1999-2016', *J. Rural Health* **36**(3), 410–415.
- Centers for Disease Control and Prevention (2023), 'National Diabetes Statistics Report website'. Accessed 2023-05-10.
URL: <https://www.cdc.gov/diabetes/data/statistics-report/index.html>
- Chu, K. Y., Lau, T., Carlsson, P.-O. and Leung, P. S. (2006), 'Angiotensin ii type 1 receptor blockade improves β -cell function and glucose tolerance in a mouse model of type 2 diabetes', *Diabetes* **55**(2), 367–374.
- Doherty, A., Jackson, D., Hammerla, N., Plötz, T., Olivier, P., Granat, M. H., White, T., Van Hees, V. T., Trenell, M. I., Owen, C. G. et al. (2017), 'Large scale population assessment of physical activity using wrist worn accelerometers: the uk biobank study', *PloS one* **12**(2), e0169649.
- Eddelbuettel, D. and Francois, R. (2011), 'Rcpp: Seamless R and C++ Integration', *Journal of Statistical Software* **40**, 1–18.
- Faletto, G. and Bien, J. (2022), 'Cluster stability selection'. preprint, arXiv:2201.00494 [stat.ME].
- Foster, G. D., Sanders, M. H., Millman, R., Zammit, G., Borradaile, K. E., Newman, A. B., Wadden, T. A., Kelley, D., Wing, R. R., Sunyer, F. X. P., Darcey, V., Kuna, S. T. and Sleep AHEAD Research Group (2009), 'Obstructive sleep apnea among obese patients with type 2 diabetes', *Diabetes Care* **32**(6), 1017–1019.
- Gaynanova, I. (2022), 'Digital biomarkers of glucose control - reproducibility challenges and opportunities', *Biopharmaceutical Report* **29**(1), 21–26.
- Gaynanova, I., Punjabi, N. and Crainiceanu, C. (2022), 'Modeling continuous glucose monitoring (CGM) data during sleep', *Biostatistics* **23**(1), 223–239.
- German, C. A., Sinsheimer, J. S., Zhou, J. and Zhou, H. (2022), 'WiSER: Robust and scalable estimation and inference of within-subject variances from intensive longitudinal data', *Biometrics* **78**(4), 1313–1327.
- Ghosal, R., Varma, V. R., Volfson, D., Hillel, I., Urbanek, J., Hausdorff, J. M., Watts, A. and Zipunnikov, V. (2021), 'Distributional data analysis via quantile functions and its application to modeling digital biomarkers of gait in Alzheimer's Disease', *Biostatistics* p. kxab041.
- Goldfarb, D. and Idnani, A. (1983), 'A numerically stable dual method for solving strictly convex quadratic programs', *Mathematical Programming* **27**(1), 1–33.
- Huang, J.-H., Lin, Y.-K., Lee, T.-W., Liu, H.-W., Chien, Y.-M., Hsueh, Y.-C., Lee, T.-I. and Chen, Y.-J. (2021), 'Correlation between short- and mid-term hemoglobin A1c and glycemic control determined by continuous glucose monitoring', *Diabetology & Metabolic Syndrome* **13**(1), 94.

- Jonas, D. E., Crotty, K., Yun, J. D. Y., Middleton, J. C., Feltner, C., Taylor-Phillips, S., Barclay, C., Dotson, A., Baker, C., Balio, C. P., Voisin, C. E. and Harris, R. P. (2021), ‘Screening for prediabetes and type 2 diabetes: Updated evidence report and systematic review for the US preventive services task force’, *JAMA* **326**(8), 744–760.
- Kodl, C. T. and Seaquist, E. R. (2008), ‘Cognitive dysfunction and diabetes mellitus’, *Endocr. Rev.* **29**(4), 494–511.
- Lam, D. C. L., Lui, M. M. S., Lam, J. C. M., Ong, L. H. Y., Lam, K. S. L. and Ip, M. S. M. (2010), ‘Prevalence and recognition of obstructive sleep apnea in chinese patients with type 2 diabetes mellitus’, *Chest* **138**(5), 1101–1107.
- Law, G. R., Ellison, G. T. H., Secher, A. L., Damm, P., Mathiesen, E. R., Temple, R., Murphy, H. R. and Scott, E. M. (2015), ‘Analysis of continuous glucose monitoring in pregnant women with diabetes: Distinct temporal patterns of glucose associated with large-for-gestational-age infants’, *Diabetes Care* **38**(7), 1319–1325.
- Li, Q., McKenzie, D. and Yin, W. (2023), ‘From the simplex to the sphere: faster constrained optimization using the Hadamard parametrization’, *Information and Inference: A Journal of the IMA* **12**(3), 1898–1937.
- Lindberg, E., Theorell-Haglöw, J., Svensson, M., Gislason, T., Berne, C. and Janson, C. (2012), ‘Sleep apnea and glucose metabolism: a long-term follow-up in a community-based sample’, *Chest* **142**(4), 935–942.
- Matabuena, M. and Petersen, A. (2023), ‘Distributional data analysis of accelerometer data from the NHANES database using nonparametric survey regression models’, *Journal of the Royal Statistical Society Series C: Applied Statistics* **72**(2), 294–313.
- Matabuena, M., Petersen, A., Vidal, J. C. and Gude, F. (2021), ‘Glucodensities: A new representation of glucose profiles using distributional data analysis’, *Stat. Methods Med. Res.* **30**(6), 1445–1464.
- Meinshausen, N. and Bühlmann, P. (2010), ‘Stability selection’, *Journal of the Royal Statistical Society: Series B (Statistical Methodology)* **72**(4), 417–473.
- Mersmann, O. (2023), ‘microbenchmark: Accurate timing functions’. R package version 1.4.10.
URL: <https://CRAN.R-project.org/package=microbenchmark>
- Mortazavi-Jahromi, S. S., Alizadeh, S., Javanbakht, M. H. and Mirshafiey, A. (2019), ‘Anti-diabetic effect of β -d-mannuronic acid (m2000) as a novel nsaid with immunosuppressive property on insulin production, blood glucose, and inflammatory markers in the experimental diabetes model’, *Archives of physiology and biochemistry* **125**(5), 435–440.
- Moxey, P. W., Gogalniceanu, P., Hinchliffe, R. J., Loftus, I. M., Jones, K. J., Thompson, M. M. and Holt, P. J. (2011), ‘Lower extremity amputations—a review of global variability in incidence’, *Diabet. Med.* **28**(10), 1144–1153.
- Petersen, A. and Müller, H.-G. (2019), ‘Fréchet regression for random objects with Euclidean predictors’, *The Annals of Statistics* **47**(2), 691 – 719.
- Petersen, A., Zhang, C. and Kokoszka, P. (2022), ‘Modeling Probability Density Functions as Data Objects’, *Econometrics and Statistics* **21**, 159–178.

- Punjabi, N. M., Sorkin, J. D., Katzel, L. I., Goldberg, A. P., Schwartz, A. R. and Smith, P. L. (2002), ‘Sleep-disordered breathing and insulin resistance in middle-aged and overweight men’, *Am. J. Respir. Crit. Care Med.* **165**(5), 677–682.
- Resnick, H. E. and Howard, B. V. (2002), ‘Diabetes and cardiovascular disease’, *Annu. Rev. Med.* **53**(1), 245–267.
- Reutrakul, S. and Mokhlesi, B. (2017), ‘Obstructive sleep apnea and diabetes: A state of the art review’, *Chest* **152**(5), 1070–1086.
- Rooney, M. R., Aurora, R. N., Wang, D., Selvin, E. and Punjabi, N. M. (2021), ‘Rationale and design of the hyperglycemic profiles in obstructive sleep apnea (HYPNOS) trial’, *Contemp. Clin. Trials* **101**(106248), 106248.
- Rosenquist, K. J. and Fox, C. S. (2018), Mortality trends in type 2 diabetes, in C. C. Cowie, S. S. Casagrande, A. Menke, M. A. Cissell, M. S. Eberhardt, J. B. Meigs, E. W. Gregg, W. C. Knowler, E. Barrett-Connor, D. J. Becker, F. L. Brancati, E. J. Boyko, W. H. Herman, B. V. Howard, K. M. V. Narayan, M. Rewers and J. E. Fradkin, eds, ‘Diabetes in America’, 3 edn, National Institute of Diabetes and Digestive and Kidney Diseases, chapter 36, pp. 36:1–14.
- Scott, E. M., Feig, D. S., Murphy, H. R., Law, G. R. and CONCEPTT Collaborative Group (2020), ‘Continuous glucose monitoring in pregnancy: Importance of analyzing temporal profiles to understand clinical outcomes’, *Diabetes Care* **43**(6), 1178–1184.
- Sergazinov, R., Leroux, A., Cui, E., Crainiceanu, C., Aurora, R. N., Punjabi, N. M. and Gaynanova, I. (2023), ‘A case study of glucose levels during sleep using multilevel fast function on scalar regression inference’, *Biometrics* **79**(4), 3873–3882.
- Shah, R. D. and Samworth, R. J. (2013), ‘Variable selection with error control: another look at stability selection’, *Journal of the Royal Statistical Society. Series B (Statistical Methodology)* **75**(1), 55–80.
- Singh, A., Chaudhary, S. C., Gupta, K. K., Sawlani, K. K., Singh, A., Singh, A. B. and Verma, A. K. (2021), ‘Prevalence of obstructive sleep apnea in diabetic patients’, *Ann. Afr. Med.* **20**(3), 206–211.
- Sobrin, L., Green, T., Sim, X., Jensen, R. A., Tai, E. S., Tay, W. T., Wang, J. J., Mitchell, P., Sandholm, N., Liu, Y., Hietala, K., Iyengar, S. K., Family Investigation of Nephropathy and Diabetes-Eye Research Group, Brooks, M., Buraczynska, M., Van Zuydam, N., Smith, A. V., Gudnason, V., Doney, A. S. F., Morris, A. D., Leese, G. P., Palmer, C. N. A., Wellcome Trust Case Control Consortium 2, Swaroop, A., Taylor, Jr, H. A., Wilson, J. G., Penman, A., Chen, C. J., Groop, P.-H., Saw, S.-M., Aung, T., Klein, B. E., Rotter, J. I., Siscovick, D. S., Cotch, M. F., Klein, R., Daly, M. J. and Wong, T. Y. (2011), ‘Candidate gene association study for diabetic retinopathy in persons with type 2 diabetes: the candidate gene association resource (CARE)’, *Invest. Ophthalmol. Vis. Sci.* **52**(10), 7593–7602.
- Tucker, D. C., Wu, Y. and Müller, H.-G. (2023), ‘Variable selection for global fréchet regression’, *Journal of the American Statistical Association* **118**(542), 1023–1037.
- Turlach, B. A., Weingessel, A. and Moler, C. (2019), ‘quadprog: Functions to solve quadratic programming problems’. R package version 1.5-8.
URL: <https://CRAN.R-project.org/package=quadprog>

- Wang, J.-L., Chiou, J.-M. and Müller, H.-G. (2016), ‘Functional Data Analysis’, *Annual Review of Statistics and Its Application* **3**(1), 257–295.
- Wu, Y. (2021), ‘Can’t ridge regression perform variable selection?’, *Technometrics* **63**(2), 263–271.

SUPPLEMENTARY MATERIAL TO

“Fast variable selection for distributional regression with application to continuous glucose monitoring data”

Abstract

This Supplementary Material is structured as follows: Supplement S1 gives supporting lemmas and proofs; Supplement S2 gives proofs of propositions in the main text; Supplement S3 describes in more detail how matrix multiplication can be avoided in the embedded problem algorithm; Supplement S4 describes our implementation of geodesic descent to efficiently scale in n and p , via algebraic manipulation of the gradient objects to avoid handling matrices of size $n \times n$ (in the $n \gg p$ case) or size $p \times p$ (in the $p \gg n$ case); Supplement S5 details the algorithms used in this paper, including modified coordinate descent (MCD) of [Tucker et al. \(2023\)](#), our geodesic second-order descent (GSD) algorithm, and our KKT multipliers method for the embedded problem; Supplement S6 details the HYPNOS dataset we analyzed in this paper.

S1 Supplementary Lemmas

Lemma S.1. *For functions $f(\lambda) : \mathbb{R} \rightarrow \mathbb{R}$ and $\mathcal{F}(\gamma) = \gamma^2 : \mathbb{R} \rightarrow \mathbb{R}$, the derivative of the composite function $g(\gamma) := (f \circ \mathcal{F})(\gamma)$ with respect to γ is*

$$\frac{d}{d\gamma}g(\gamma) = 2\gamma \cdot \frac{d}{d\lambda}f(\lambda).$$

Proof. This follows immediately from the chain rule

$$\frac{d}{d\gamma}g(\gamma) = \frac{d}{d\gamma}(f \circ \mathcal{F})(\gamma) = \frac{d}{d\lambda}f(\lambda) \cdot \frac{d}{d\gamma}\mathcal{F}(\gamma) = \frac{d}{d\gamma}\gamma^2 \cdot \frac{d}{d\lambda}f(\lambda) = 2\gamma \cdot \frac{d}{d\lambda}f(\lambda). \quad \square$$

Lemma S.2. *Let $\underline{\mathbf{u}}$ and $\underline{\mathbf{v}}$ be orthonormal vectors in \mathbb{R}^p , $p \geq 2$. Then the unique matrix which rotates $\underline{\mathbf{u}} \rightarrow \underline{\mathbf{v}}$ by angle $\theta \in \mathbb{R}$, while fixing the orthogonal complement of $\text{span}\{\underline{\mathbf{u}}, \underline{\mathbf{v}}\}$, is*

$$\mathbf{R}_\theta = \mathbf{I}_p + (\sin \theta)(\underline{\mathbf{v}}\underline{\mathbf{u}}^\top - \underline{\mathbf{u}}\underline{\mathbf{v}}^\top) + (\cos \theta - 1)(\underline{\mathbf{u}}\underline{\mathbf{u}}^\top + \underline{\mathbf{v}}\underline{\mathbf{v}}^\top). \quad (\text{S1})$$

Proof. We prove this in parts.

1. **\mathbf{R}_θ is a proper rotation matrix:**

A matrix \mathbf{R} is a proper rotation matrix iff $\mathbf{R}^\top = \mathbf{R}^{-1}$ and $|\mathbf{R}| = 1$. We start with $\mathbf{R}_\theta^\top \mathbf{R}_\theta$

$$\mathbf{R}_\theta^\top \mathbf{R}_\theta = \mathbf{R}_\theta^\top \mathbf{I}_p + (\sin \theta) \mathbf{R}_\theta^\top (\underline{\mathbf{v}}\underline{\mathbf{u}}^\top - \underline{\mathbf{u}}\underline{\mathbf{v}}^\top) + (\cos \theta - 1) \mathbf{R}_\theta^\top (\underline{\mathbf{u}}\underline{\mathbf{u}}^\top + \underline{\mathbf{v}}\underline{\mathbf{v}}^\top).$$

The first term is

$$\mathbf{R}_\theta^\top \mathbf{I}_p = \mathbf{I}_p + (\sin \theta)(\underline{\mathbf{u}}\underline{\mathbf{v}}^\top - \underline{\mathbf{v}}\underline{\mathbf{u}}^\top) + (\cos \theta - 1)(\underline{\mathbf{u}}\underline{\mathbf{u}}^\top + \underline{\mathbf{v}}\underline{\mathbf{v}}^\top).$$

The second term is

$$\begin{aligned}
(\sin \theta) \mathbf{R}_\theta^\top (\underline{\mathbf{v}} \underline{\mathbf{u}}^\top - \underline{\mathbf{u}} \underline{\mathbf{v}}^\top) &= (\sin \theta) (\underline{\mathbf{v}} \underline{\mathbf{u}}^\top - \underline{\mathbf{u}} \underline{\mathbf{v}}^\top) + \sin^2 \theta (\underline{\mathbf{u}} \underline{\mathbf{v}}^\top - \underline{\mathbf{v}} \underline{\mathbf{u}}^\top) (\underline{\mathbf{v}} \underline{\mathbf{u}}^\top - \underline{\mathbf{u}} \underline{\mathbf{v}}^\top) + \\
&\quad (\sin \theta) (\cos \theta - 1) (\underline{\mathbf{u}} \underline{\mathbf{u}}^\top + \underline{\mathbf{v}} \underline{\mathbf{v}}^\top) (\underline{\mathbf{v}} \underline{\mathbf{u}}^\top - \underline{\mathbf{u}} \underline{\mathbf{v}}^\top) \\
&= (\sin \theta) (\underline{\mathbf{v}} \underline{\mathbf{u}}^\top - \underline{\mathbf{u}} \underline{\mathbf{v}}^\top) + \sin^2 \theta (\underline{\mathbf{u}} \underline{\mathbf{u}}^\top + \underline{\mathbf{v}} \underline{\mathbf{v}}^\top) + \\
&\quad (\sin \theta) (\cos \theta - 1) (\underline{\mathbf{v}} \underline{\mathbf{u}}^\top - \underline{\mathbf{u}} \underline{\mathbf{v}}^\top) \\
&= \sin^2 \theta (\underline{\mathbf{u}} \underline{\mathbf{u}}^\top + \underline{\mathbf{v}} \underline{\mathbf{v}}^\top) + (\sin \theta \cos \theta) (\underline{\mathbf{v}} \underline{\mathbf{u}}^\top - \underline{\mathbf{u}} \underline{\mathbf{v}}^\top).
\end{aligned}$$

The third term is

$$\begin{aligned}
(\cos \theta - 1) \mathbf{R}_\theta^\top (\underline{\mathbf{u}} \underline{\mathbf{u}}^\top + \underline{\mathbf{v}} \underline{\mathbf{v}}^\top) &= (\cos \theta - 1) (\underline{\mathbf{u}} \underline{\mathbf{u}}^\top + \underline{\mathbf{v}} \underline{\mathbf{v}}^\top) + (\cos \theta - 1)^2 (\underline{\mathbf{u}} \underline{\mathbf{u}}^\top + \underline{\mathbf{v}} \underline{\mathbf{v}}^\top)^2 + \\
&\quad (\sin \theta) (\cos \theta - 1) (\underline{\mathbf{u}} \underline{\mathbf{v}}^\top - \underline{\mathbf{v}} \underline{\mathbf{u}}^\top) (\underline{\mathbf{u}} \underline{\mathbf{u}}^\top + \underline{\mathbf{v}} \underline{\mathbf{v}}^\top) \\
&= (\cos \theta - 1 + \cos^2 \theta - 2 \cos \theta + 1) (\underline{\mathbf{u}} \underline{\mathbf{u}}^\top + \underline{\mathbf{v}} \underline{\mathbf{v}}^\top) + \\
&\quad (\sin \theta) (\cos \theta - 1) (\underline{\mathbf{u}} \underline{\mathbf{v}}^\top - \underline{\mathbf{v}} \underline{\mathbf{u}}^\top) \\
&= (\cos^2 \theta - \cos \theta) (\underline{\mathbf{u}} \underline{\mathbf{u}}^\top + \underline{\mathbf{v}} \underline{\mathbf{v}}^\top) + \\
&\quad (\sin \theta) (\cos \theta - 1) (\underline{\mathbf{u}} \underline{\mathbf{v}}^\top - \underline{\mathbf{v}} \underline{\mathbf{u}}^\top).
\end{aligned}$$

Matching pieces by their trigonometric constants, and using identity $\cos^2 \theta + \sin^2 \theta = 1$, we see all terms except for \mathbf{I}_p cancel, hence $\mathbf{R}_\theta^\top \mathbf{R}_\theta = \mathbf{I}_p$. A nearly identical argument shows $\mathbf{R}_\theta \mathbf{R}_\theta^\top = \mathbf{I}_p$, hence $\mathbf{R}_\theta^\top = \mathbf{R}_\theta^{-1}$.

It follows $|\mathbf{R}_\theta| = \pm 1$. Note however the eigenvalues of $(\sin \theta) (\underline{\mathbf{v}} \underline{\mathbf{u}}^\top - \underline{\mathbf{u}} \underline{\mathbf{v}}^\top)$ are zero except for two complex conjugates, and the eigenvalues of $(\cos \theta - 1) (\underline{\mathbf{u}} \underline{\mathbf{u}}^\top + \underline{\mathbf{v}} \underline{\mathbf{v}}^\top)$ are zero except for two identical (negative real) values. Since the eigenspaces of these terms are both $\text{span}(\underline{\mathbf{u}}, \underline{\mathbf{v}})$, the rank of $\mathbf{R}_\theta - \mathbf{I}_p$ is also 2, with eigenvalues also zero except for two complex conjugates. Adding back \mathbf{I}_p , the product of the eigenvalues of \mathbf{R}_θ (i.e. its determinant) must then be positive—specifically, $+1$ —hence \mathbf{R}_θ is a proper rotation matrix.

2. **\mathbf{R}_θ rotates $\underline{\mathbf{u}} \rightarrow \underline{\mathbf{v}}$ by angle θ :**

For $\theta > 0$, the matrix \mathbf{R}_θ applied to $\underline{\mathbf{u}}$ gives

$$\begin{aligned}
\mathbf{R}_\theta \underline{\mathbf{u}} &= \underline{\mathbf{u}} + (\sin \theta) (\underline{\mathbf{v}} \underline{\mathbf{u}}^\top - \underline{\mathbf{u}} \underline{\mathbf{v}}^\top) \underline{\mathbf{u}} + (\cos \theta - 1) (\underline{\mathbf{u}} \underline{\mathbf{u}}^\top + \underline{\mathbf{v}} \underline{\mathbf{v}}^\top) \underline{\mathbf{u}} \\
&= \underline{\mathbf{u}} + (\sin \theta) (\underline{\mathbf{v}}) + (\cos \theta - 1) (\underline{\mathbf{u}}) \\
&= (\cos \theta) (\underline{\mathbf{u}}) + (\sin \theta) (\underline{\mathbf{v}}).
\end{aligned}$$

Clearly for any θ , the angle between $\mathbf{R}_\theta \underline{\mathbf{u}}$ and $\underline{\mathbf{u}}$ is θ ; in particular for $\theta = \pi/2$, $\mathbf{R}_\theta \underline{\mathbf{u}} = \underline{\mathbf{v}}$.

3. **\mathbf{R}_θ fixes the orthogonal complement of $\text{span}(\underline{\mathbf{u}}, \underline{\mathbf{v}})$:**

Clearly for any $\mathbf{z} \perp \text{span}(\underline{\mathbf{u}}, \underline{\mathbf{v}})$

$$\mathbf{R}_\theta \mathbf{z} = \{\mathbf{I}_p + (\sin \theta) (\underline{\mathbf{v}} \underline{\mathbf{u}}^\top - \underline{\mathbf{u}} \underline{\mathbf{v}}^\top) + (\cos \theta - 1) (\underline{\mathbf{u}} \underline{\mathbf{u}}^\top + \underline{\mathbf{v}} \underline{\mathbf{v}}^\top)\} \mathbf{z} = \mathbf{I}_p \mathbf{z} + \mathbf{0} + \mathbf{0} = \mathbf{z}.$$

4. **\mathbf{R}_θ is unique:**

Suppose \mathbf{R}_* performs the same rotation operation as \mathbf{R}_θ , i.e. $\mathbf{R}_* \mathbf{z} = \mathbf{R}_\theta \mathbf{z}$ for all $\mathbf{z} \in \mathbb{R}^p$. Then $(\mathbf{R}_* - \mathbf{R}_\theta) \mathbf{z} = \mathbf{0}_p$ for all \mathbf{z} ; but this is only true if $\mathbf{R}_* - \mathbf{R}_\theta = \mathbf{0} \iff \mathbf{R}_* = \mathbf{R}_\theta$. \square

S2 Proofs of Propositions

Proof of Proposition 3.1

Let $\mathbf{X} \in \mathbb{R}^{n \times p}$ be a column-centered variable matrix, $\mathbf{x}_* \in \mathbb{R}^p$ be a vector centered the same as \mathbf{X} , and let $\mathbf{Y} \in \mathbb{R}^{n \times m}$ be a matrix holding a set of empirical quantile functions defined on a shared, uniformly dispersed m -grid in $(0, 1)$. The estimated conditional Fréchet mean $\hat{\mathbf{q}}_* \equiv \hat{\mathbf{q}}(\mathbf{x}_*)$ is the solution to the optimization problem

$$\hat{\mathbf{q}}_* := \arg \min_{\mathbf{q} \in \mathbb{R}^m} \sum_{i=1}^n s_i(\mathbf{x}_*) \|\mathbf{q} - \mathbf{y}_i\|_2^2, \quad \text{subject to} \quad \mathbf{b} - \mathbf{A}^\top \mathbf{q} \leq \mathbf{0}_a, \quad (\text{S2})$$

where $s_i(\mathbf{x}_*) = \frac{1}{n} + \mathbf{x}_*^\top (\mathbf{X}^\top \mathbf{X})^{-1} \mathbf{x}_i$. The objective function can be rewritten

$$\begin{aligned} \sum_{i=1}^n s_i(\mathbf{x}_*) \|\mathbf{q} - \mathbf{y}_i\|_2^2 &= \sum_{i=1}^n s_i(\mathbf{x}_*) \sum_{j=1}^m (y_{i,j} - q_j)^2 \\ &= \sum_{i=1}^n s_i(\mathbf{x}_*) \sum_{j=1}^m (y_{i,j}^2 - 2y_{i,j}q_j + q_j^2) \\ &= \sum_{j=1}^m \left[\left(\sum_{i=1}^n s_i(\mathbf{x}_*) y_{i,j}^2 \right) - 2 \left(q_j \sum_{i=1}^n s_i(\mathbf{x}_*) y_{i,j} \right) + \left(q_j^2 \sum_{i=1}^n s_i(\mathbf{x}_*) \right) \right] \\ &= \kappa + \mathbf{q}^\top \mathbf{q} - 2\mathbf{q}^\top \hat{\mathbf{y}}_*, \end{aligned}$$

where κ is a constant free of \mathbf{q} , and $\hat{\mathbf{y}}_*^\top = (n^{-1} \mathbf{1}_n^\top + \mathbf{x}_*^\top (\mathbf{X}^\top \mathbf{X})^{-1} \mathbf{X}^\top) \mathbf{Y}$. Then since the arg min is invariant to κ and to scaling, we have

$$\hat{\mathbf{q}}_* = \arg \min_{\mathbf{q} \in \mathbb{R}^m} \frac{1}{2} \|\mathbf{q} - \hat{\mathbf{y}}_*\|_2^2, \quad \text{subject to} \quad \mathbf{b} - \mathbf{A}^\top \mathbf{q} \leq \mathbf{0}_a. \quad (\text{S3})$$

This proves the first part of the proposition. Let $\mathbf{X}_* \in \mathbb{R}^{d \times p}$ be a matrix of variable vectors column-centered as \mathbf{X} , and $\hat{\mathbf{Q}}_* \in \mathbb{R}^{d \times m}$ the matrix row-wise consisting of the solutions to (S3). Since Frobenius norm is element-wise, the joint result follows immediately by row-adjoining

$$\hat{\mathbf{Q}}_* := \arg \min_{\mathbf{Q} \in \mathbb{R}^{d \times m}} \|\mathbf{Q} - \hat{\mathbf{Y}}_*\|_F^2, \quad \text{subject to} \quad \mathbf{B} - \mathbf{Q}\mathbf{A} \leq \mathbf{0}_{d \times (m+1)},$$

where the rows of \mathbf{B} are each \mathbf{b} , and $\hat{\mathbf{Y}}_* := (n^{-1} \mathbf{1}_{d \times n} + \mathbf{X}_* (\mathbf{X}^\top \mathbf{X})^{-1} \mathbf{X}^\top) \mathbf{Y}$.

Proof of Proposition 4.1

The objective function of (7) is

$$f(\boldsymbol{\lambda}) = \frac{1}{2} \|\mathbf{Y} - \hat{\mathbf{Q}}(\boldsymbol{\lambda})\|_F^2, \quad \text{subject to} \quad \boldsymbol{\lambda} \in \mathbf{T}, \quad (\text{S4})$$

where

$$\hat{\mathbf{Q}}(\boldsymbol{\lambda}) = \arg \min_{\mathbf{Q} \in \mathbb{R}^{n \times m}} \|\mathbf{Q} - \hat{\mathbf{Y}}(\boldsymbol{\lambda})\|_F^2, \quad \text{subject to} \quad \mathbf{B} - \mathbf{Q}\mathbf{A} \leq \mathbf{0}_{n \times (m+1)},$$

and

$$\hat{\mathbf{Y}}(\boldsymbol{\lambda}) = n^{-1} \mathbf{1}_{n \times n} \mathbf{Y} + \tilde{\mathbf{X}}(\tilde{\mathbf{X}}^\top \tilde{\mathbf{X}} + \mathbf{D}_\lambda^{-1})^{-1} \tilde{\mathbf{X}}^\top \mathbf{Y}.$$

To prevent division by zero, note we can rewrite this matrix using the push-through identity

$$\begin{aligned} \hat{\mathbf{Y}}(\boldsymbol{\lambda}) &= n^{-1} \mathbf{1}_{n \times n} \mathbf{Y} + \tilde{\mathbf{X}} \mathbf{D}_\lambda^{1/2} (\mathbf{D}_\lambda^{1/2} \tilde{\mathbf{X}}^\top \tilde{\mathbf{X}} \mathbf{D}_\lambda^{1/2} + \mathbf{I}_p)^{-1} \mathbf{D}_\lambda^{1/2} \tilde{\mathbf{X}}^\top \mathbf{Y} \\ &= n^{-1} \mathbf{1}_{n \times n} \mathbf{Y} + \tilde{\mathbf{X}} \mathbf{D}_\lambda \tilde{\mathbf{X}}^\top (\tilde{\mathbf{X}} \mathbf{D}_\lambda \tilde{\mathbf{X}}^\top + \mathbf{I}_n)^{-1} \mathbf{Y} \\ &= n^{-1} \mathbf{1}_{n \times n} \mathbf{Y} + \mathbf{Y} - (\tilde{\mathbf{X}} \mathbf{D}_\lambda \tilde{\mathbf{X}}^\top + \mathbf{I}_n)^{-1} \mathbf{Y}. \end{aligned}$$

We define $\mathbf{G} \equiv \mathbf{G}(\boldsymbol{\lambda}) := (\tilde{\mathbf{X}} \mathbf{D}_\lambda \tilde{\mathbf{X}}^\top + \mathbf{I}_n)^{-1}$, so that

$$\hat{\mathbf{Y}}(\boldsymbol{\lambda}) = n^{-1} \mathbf{1}_{n \times n} \mathbf{Y} + \mathbf{Y} - \mathbf{G} \mathbf{Y}. \quad (\text{S5})$$

Let $\hat{\mathbf{Q}} = \hat{\mathbf{Q}}(\boldsymbol{\lambda})$ and $\hat{\mathbf{Y}} = \hat{\mathbf{Y}}(\boldsymbol{\lambda})$. The partial derivative of (S4) with respect to λ_k is:

$$\frac{\partial}{\partial \lambda_k} f(\boldsymbol{\lambda}) = \text{tr} \left\{ (\hat{\mathbf{Q}} - \mathbf{Y}) \left(\frac{\partial}{\partial \lambda_k} \hat{\mathbf{Q}} \right)^\top \right\}. \quad (\text{S6})$$

To evaluate the partial derivative of $\hat{\mathbf{Q}}$, consider the optimality conditions associated with (8). The optimal $\hat{\mathbf{Q}}$, with corresponding optimal Lagrange multiplier $\hat{\mathbf{H}} \in \mathbb{R}^{n \times (m+1)}$, satisfy KKT conditions of stationarity of the associated Lagrangian

$$\frac{\partial}{\partial \mathbf{Q}} \mathcal{L}(\hat{\mathbf{Q}}, \hat{\mathbf{H}}) := \frac{\partial}{\partial \mathbf{Q}} \left[\|\mathbf{Q} - \hat{\mathbf{Y}}\|_F^2 + \text{tr} \{ (\mathbf{B} - \mathbf{Q} \mathbf{A}) \mathbf{H}^\top \} \right] \Big|_{\hat{\mathbf{Q}}, \hat{\mathbf{H}}} = \hat{\mathbf{Q}} - \hat{\mathbf{Y}} - \hat{\mathbf{H}} \mathbf{A}^\top = \mathbf{0}_{n \times m} \quad (\text{S7})$$

and complementary slackness

$$(\mathbf{B} - \hat{\mathbf{Q}} \mathbf{A}) \circ \hat{\mathbf{H}} = \mathbf{0}_{n \times (m+1)}. \quad (\text{S8})$$

Denote $\mathbf{Q} := \frac{\partial}{\partial \lambda_k} \hat{\mathbf{Q}}$, $\mathbf{H} := \frac{\partial}{\partial \lambda_k} \hat{\mathbf{H}}$, and $\mathbf{Y} := \frac{\partial}{\partial \lambda_k} \hat{\mathbf{Y}}$. Applying the partial derivative operator to each of (S7) and (S8), we respectively obtain:

$$\frac{\partial}{\partial \lambda_k} (\hat{\mathbf{Q}} - \hat{\mathbf{Y}} - \hat{\mathbf{H}} \mathbf{A}^\top) = \frac{\partial}{\partial \lambda_k} \mathbf{0}_{n \times m} \iff \mathbf{Q} - \mathbf{Y} - \mathbf{H} \mathbf{A}^\top = \mathbf{0}_{n \times m}, \quad (\text{S9})$$

and:

$$\frac{\partial}{\partial \lambda_k} \{ (\mathbf{B} - \hat{\mathbf{Q}} \mathbf{A}) \circ \hat{\mathbf{H}} \} = \frac{\partial}{\partial \lambda_k} \mathbf{0}_{n \times (m+1)} \iff (\mathbf{B} - \hat{\mathbf{Q}} \mathbf{A}) \circ \mathbf{H} = (\mathbf{Q} \mathbf{A}) \circ \hat{\mathbf{H}} \quad (\text{S10})$$

From (S9), our desired \mathbf{Q} is a function of two other gradients \mathbf{Y} and \mathbf{H} which we find next.

First, using (S5) and recalling $\partial_x \mathbf{M}^{-1}(x) = -\mathbf{M}^{-1}(x) \{ \partial_x \mathbf{M}(x) \} \mathbf{M}^{-1}(x)$, we have

$$\mathbf{Y} = \frac{\partial}{\partial \lambda_k} (n^{-1} \mathbf{1}_{n \times n} \mathbf{Y} + \mathbf{Y} - \mathbf{G} \mathbf{Y}) = -\frac{\partial}{\partial \lambda_k} (\tilde{\mathbf{X}} \mathbf{D}_\lambda \tilde{\mathbf{X}}^\top + \mathbf{I}_n)^{-1} \mathbf{Y} = \mathbf{G} \tilde{\mathbf{X}}_k \tilde{\mathbf{X}}_k^\top \mathbf{G} \mathbf{Y}. \quad (\text{S11})$$

To evaluate the gradient \mathbf{H} , let $\mathbf{C} := \mathbf{B} - \hat{\mathbf{Q}} \mathbf{A}$ be the constraint matrix associated with $\hat{\mathbf{Q}}$, where zero-valued entries indicate active constraints. Consider two cases: element-wise, if $c_{i,\ell} < 0$, then by (S8) we have

$\hat{h}_{i,\ell} = 0$, which through (S10) implies $\eta_{i,\ell} = 0$; on the other hand, if $c_{i,\ell} = 0$, then using (S9) for \mathcal{Q}

$$[B - \hat{\mathcal{Q}}\mathbf{A}]_{i,\ell} = 0 \quad \Rightarrow \quad \frac{\partial}{\partial \lambda_k} b_{i,\ell} = [\mathcal{Q}\mathbf{A}]_{i,\ell} \iff 0 = [\mathcal{Y}\mathbf{A} + \mathcal{H}\mathbf{A}^\top \mathbf{A}]_{i,\ell}.$$

The constraint matrix \mathbf{C} then implicates the derivative matrix $\mathcal{H} = [\eta_{i,\ell}]$ in the system of equations

$$\begin{aligned} c_{i,\ell} = 0 &\Rightarrow [\mathcal{H}\mathbf{A}^\top \mathbf{A}]_{i,\ell} = -[\mathcal{Y}\mathbf{A}]_{i,\ell}, \\ c_{i,\ell} < 0 &\Rightarrow \eta_{i,\ell} = 0. \end{aligned} \tag{S12}$$

This system can be solved independently for rows of \mathcal{H} . Denote the i^{th} rows of \mathcal{H} , \mathcal{Y} , and \mathbf{C} with $\boldsymbol{\eta}_i = (\eta_{i,1} \ \cdots \ \eta_{i,m+1})^\top$, $\mathbf{y}_i = (y_{i,1} \ \cdots \ y_{i,m+1})^\top$, and $\mathbf{c}_i = (c_{i,1} \ \cdots \ c_{i,m+1})^\top$, respectively. If $\mathbf{c}_i < \mathbf{0}$, then we take $\boldsymbol{\eta}_i = \mathbf{0}$. The case $\mathbf{c}_i = \mathbf{0}$ is not possible, as it implies all constraints are active for $\hat{\mathbf{q}}_i$, namely the quantile function is constant and equal to both box constraints b_L, b_U . But this gives rise to a contradiction since $b_L < b_U$ for the support.

The remaining case is where some elements of \mathbf{c}_i are zero (active constraints) and some are negative (inactive constraints). Without loss of generality, let $\mathbf{A} = [\mathbf{A}_{0,i} \ \mathbf{A}_{-,i}]$ be the block decomposition of \mathbf{A} into those columns corresponding to the i^{th} active constraints (i.e. $\mathbf{A}_{0,i}$) and the i^{th} inactive constraints (i.e. $\mathbf{A}_{-,i}$), with $\boldsymbol{\eta}_i^\top = [\boldsymbol{\eta}_{0,i}^\top \ \boldsymbol{\eta}_{-,i}^\top]$ split analogously. The i^{th} system from (S12) is

$$\begin{bmatrix} \mathbf{A}_{0,i}^\top \mathbf{A}_{0,i} & \mathbf{A}_{0,i}^\top \mathbf{A}_{-,i} \\ \mathbf{0} & \mathbf{I} \end{bmatrix} \begin{bmatrix} \boldsymbol{\eta}_{0,i} \\ \boldsymbol{\eta}_{-,i} \end{bmatrix} = - \begin{bmatrix} \mathbf{A}_{0,i}^\top \mathbf{y}_i \\ \mathbf{0} \end{bmatrix}$$

We immediately have $\boldsymbol{\eta}_{-,i} = \mathbf{0}$, as desired, and since $\mathbf{A}_{0,i}$ is guaranteed to be full column rank

$$\begin{aligned} \mathbf{A}_{0,i}^\top \mathbf{A}_{0,i} \boldsymbol{\eta}_{0,i} &= -\mathbf{A}_{0,i}^\top \mathbf{y}_i \\ \boldsymbol{\eta}_{0,i} &= -(\mathbf{A}_{0,i}^\top \mathbf{A}_{0,i})^{-1} \mathbf{A}_{0,i}^\top \mathbf{y}_i. \end{aligned}$$

With the solution for each i^{th} row of \mathcal{H} , recall from (S9) that $\mathcal{Q} = \mathcal{Y} + \mathcal{H}\mathbf{A}^\top$. Thus

$$\mathbf{A}\boldsymbol{\eta}_i = [\mathbf{A}_{0,i} \ \mathbf{A}_{-,i}] \begin{bmatrix} \boldsymbol{\eta}_{0,i} \\ \boldsymbol{\eta}_{-,i} \end{bmatrix} = \mathbf{A}_{0,i} \boldsymbol{\eta}_{0,i} + \mathbf{A}_{-,i} \boldsymbol{\eta}_{-,i} = \mathbf{A}_{0,i} \{ -(\mathbf{A}_{0,i}^\top \mathbf{A}_{0,i})^{-1} \mathbf{A}_{0,i}^\top \mathbf{y}_i \} + \mathbf{0} = -\mathbb{P}_{\mathbf{A}_{0,i}} \mathbf{y}_i,$$

where we interpret $\mathbb{P}_{\mathbf{A}_{0,i}} = \mathbf{0}_{m \times m}$ when $\mathbf{c}_i < \mathbf{0}$. Plugging in we get

$$\mathcal{Q} = \mathcal{Y} + \mathcal{H}\mathbf{A}^\top = \begin{bmatrix} \mathbf{y}_1^\top (\mathbf{I}_m - \mathbb{P}_{\mathbf{A}_{0,1}}) \\ \vdots \\ \mathbf{y}_n^\top (\mathbf{I}_m - \mathbb{P}_{\mathbf{A}_{0,n}}) \end{bmatrix}.$$

Plugging this back into (S6)

$$\frac{\partial}{\partial \lambda_k} f(\boldsymbol{\lambda}) = \text{tr} \left\{ (\hat{\mathcal{Q}} - \mathbf{Y}) \begin{bmatrix} \mathbf{y}_1^\top (\mathbf{I}_m - \mathbb{P}_{\mathbf{A}_{0,1}}) \\ \vdots \\ \mathbf{y}_n^\top (\mathbf{I}_m - \mathbb{P}_{\mathbf{A}_{0,n}}) \end{bmatrix}^\top \right\}. \tag{S13}$$

From (S11) we can row-wise express \mathbf{y}

$$\mathbf{y} = \begin{bmatrix} \mathbf{y}_1^\top \\ \vdots \\ \mathbf{y}_n^\top \end{bmatrix} = \begin{bmatrix} \underline{\mathbf{e}}_1^\top \mathbf{G} \tilde{\mathbf{X}}_k \tilde{\mathbf{X}}_k^\top \mathbf{G} \mathbf{Y} \\ \vdots \\ \underline{\mathbf{e}}_n^\top \mathbf{G} \tilde{\mathbf{X}}_k \tilde{\mathbf{X}}_k^\top \mathbf{G} \mathbf{Y} \end{bmatrix}.$$

Inserting these individual row vectors into (S13) we obtain

$$\begin{aligned} \frac{\partial}{\partial \lambda_k} f(\lambda) &= \text{tr} \left\{ (\hat{\mathbf{Q}} - \mathbf{Y}) \begin{bmatrix} \underline{\mathbf{e}}_1^\top \mathbf{G} \tilde{\mathbf{X}}_k \tilde{\mathbf{X}}_k^\top \mathbf{G} \mathbf{Y} (\mathbf{I}_m - \mathbb{P}_{\mathbf{A}_{0,1}}) \\ \vdots \\ \underline{\mathbf{e}}_n^\top \mathbf{G} \tilde{\mathbf{X}}_k \tilde{\mathbf{X}}_k^\top \mathbf{G} \mathbf{Y} (\mathbf{I}_m - \mathbb{P}_{\mathbf{A}_{0,n}}) \end{bmatrix}^\top \right\} \\ &= \sum_{i=1}^n \left\{ (\hat{\mathbf{q}}_i - \mathbf{y}_i)^\top (\mathbf{I}_m - \mathbb{P}_{\mathbf{A}_{0,i}}) \mathbf{Y}^\top \mathbf{G} \tilde{\mathbf{X}}_k \right\} \left\{ \tilde{\mathbf{X}}_k^\top \mathbf{G} \underline{\mathbf{e}}_i \right\} \\ &= \sum_{i=1}^n \left\{ \tilde{\mathbf{X}}_k^\top \mathbf{G} \underline{\mathbf{e}}_i \right\} \left\{ (\hat{\mathbf{q}}_i^\top - \mathbf{y}_i^\top) (\mathbf{I}_m - \mathbb{P}_{\mathbf{A}_{0,i}}) \mathbf{Y}^\top \mathbf{G} \tilde{\mathbf{X}}_k \right\} \\ &= \tilde{\mathbf{X}}_k^\top \mathbf{G} \left\{ \sum_{i=1}^n \underline{\mathbf{e}}_i (\hat{\mathbf{q}}_i^\top - \mathbf{y}_i^\top) (\mathbf{I}_m - \mathbb{P}_{\mathbf{A}_{0,i}}) \right\} \mathbf{Y}^\top \mathbf{G} \tilde{\mathbf{X}}_k. \end{aligned} \quad (\text{S14})$$

Since $\mathbf{A}_{0,i}$ are the columns of \mathbf{A} corresponding to the active constraints on $\hat{\mathbf{q}}_i$, we can rewrite the optimization problem for $\hat{\mathbf{q}}_i$ in terms of only those constraints via

$$\hat{\mathbf{q}}_i = \arg \min_{\mathbf{q}_i \in \mathbb{R}^m} \frac{1}{2} \|\mathbf{q}_i - \hat{\mathbf{y}}_i\|_2^2, \quad \text{subject to} \quad \mathbf{b}_{0,i} - \mathbf{A}_{0,i}^\top \mathbf{q}_i = \mathbf{0}.$$

The Lagrangian associated with the above objective function is

$$\mathcal{L}(\mathbf{q}_i, \beta_i) = \frac{1}{2} (\mathbf{q}_i^\top \mathbf{q}_i - 2 \mathbf{q}_i^\top \hat{\mathbf{y}}_i + \hat{\mathbf{y}}_i^\top \hat{\mathbf{y}}_i) + \beta_i^\top (\mathbf{b}_{0,i} - \mathbf{A}_{0,i}^\top \mathbf{q}_i).$$

The optimality conditions are primal feasibility and stability, given respectively by

$$\mathbf{b}_{0,i} - \mathbf{A}_{0,i}^\top \hat{\mathbf{q}}_i = \mathbf{0}, \quad \frac{\partial}{\partial \mathbf{q}_i} \mathcal{L}(\hat{\mathbf{q}}_i, \hat{\beta}_i) = \hat{\mathbf{q}}_i - \hat{\mathbf{y}}_i - \mathbf{A}_{0,i} \hat{\beta}_i = \mathbf{0}.$$

Combining these expressions, we obtain

$$\hat{\beta}_i = (\mathbf{A}_{0,i}^\top \mathbf{A}_{0,i})^{-1} (\mathbf{b}_{0,i} - \mathbf{A}_{0,i}^\top \hat{\mathbf{y}}_i), \quad \hat{\mathbf{q}}_i = (\mathbf{I}_m - \mathbb{P}_{\mathbf{A}_{0,i}}) \hat{\mathbf{y}}_i + \mathbf{A}_{0,i} (\mathbf{A}_{0,i}^\top \mathbf{A}_{0,i})^{-1} \mathbf{b}_{0,i}.$$

Plugging the expression for $\hat{\mathbf{q}}_i$ into (S14)

$$\begin{aligned} \frac{\partial}{\partial \lambda_k} f(\lambda) &= \tilde{\mathbf{X}}_k^\top \mathbf{G} \left[\sum_{i=1}^n \underline{\mathbf{e}}_i \left\{ \hat{\mathbf{y}}_i^\top (\mathbf{I}_m - \mathbb{P}_{\mathbf{A}_{0,i}}) + \mathbf{b}_{0,i}^\top (\mathbf{A}_{0,i}^\top \mathbf{A}_{0,i})^{-1} \mathbf{A}_{0,i}^\top - \mathbf{y}_i^\top \right\} (\mathbf{I}_m - \mathbb{P}_{\mathbf{A}_{0,i}}) \right] \mathbf{Y}^\top \mathbf{G} \tilde{\mathbf{X}}_k \\ &= \tilde{\mathbf{X}}_k^\top \mathbf{G} \left\{ \sum_{i=1}^n \underline{\mathbf{e}}_i (\hat{\mathbf{y}}_i^\top - \mathbf{y}_i^\top) (\mathbf{I}_m - \mathbb{P}_{\mathbf{A}_{0,i}}) \right\} \mathbf{Y}^\top \mathbf{G} \tilde{\mathbf{X}}_k \\ &= \tilde{\mathbf{X}}_k^\top \mathbf{G} \left\{ \sum_{i=1}^n \underline{\mathbf{e}}_i \underline{\mathbf{e}}_i^\top (\hat{\mathbf{Y}} - \mathbf{Y}) (\mathbf{I}_m - \mathbb{P}_{\mathbf{A}_{0,i}}) \right\} \mathbf{Y}^\top \mathbf{G} \tilde{\mathbf{X}}_k. \end{aligned} \quad (\text{S15})$$

Finally, combining across k 's, the full gradient of (S4) is

$$\nabla f(\boldsymbol{\lambda}) = \text{diag}(\mathbf{N}),$$

where

$$\mathbf{N} := \tilde{\mathbf{X}}^\top \mathbf{G} \left\{ \sum_{i=1}^n \mathbf{e}_i \mathbf{e}_i^\top (\hat{\mathbf{Y}} - \mathbf{Y})(\mathbf{I}_m - \mathbb{P}_{\mathbf{A}_{0,i}}) \right\} \mathbf{Y}^\top \mathbf{G} \tilde{\mathbf{X}}. \quad (\text{S16})$$

Before deriving the Hessian, we make two key observations. The first is that the matrices $\{\mathbb{P}_{\mathbf{A}_{0,i}}\}_{i=1}^n$ are implicitly functions of $\boldsymbol{\lambda}$, since changing $\boldsymbol{\lambda}$ can change which constraints become active or inactive on $\hat{\mathbf{Q}}$. However, as a function on the simplex \mathbf{T} , $\mathbb{P}_{\mathbf{A}_{0,i}}(\boldsymbol{\lambda})$ is piece-wise constant, since any change in the projection matrix occurs by inclusion or exclusion of new columns of \mathbf{A} . There is only a finite number of ways to select columns of \mathbf{A} to create $\mathbf{A}_{0,i}$, and so with respect to the Lebesgue measure μ , $\mu \left\{ \frac{\partial}{\partial \lambda_k} \mathbb{P}_{\mathbf{A}_{0,i}} \neq \mathbf{0} \right\} = 0$.

The second is that these points of discontinuity in $\mathbb{P}_{\mathbf{A}_{0,i}}$ over \mathbf{T} correspond to instances where the unconstrained solution $\hat{\mathbf{Y}}$ is *exactly* on the boundary specified by $\mathbf{B} - \hat{\mathbf{Y}}\mathbf{A} \leq \mathbf{0}$. From (S5), each column in $\hat{\mathbf{Y}}(\boldsymbol{\lambda})$ is a weighted mean of the corresponding column of \mathbf{Y} , so there are two scenarios under which this can happen.

- All observations in one or more columns \mathbf{Y}_j are equal to each other. Then no matter what $\boldsymbol{\lambda}$ is, the weighted mean takes the same value, and so the unconstrained solution can rest exactly on a box constraint (if all observed values lie on that box constraint) or exhibit constancy over sequential columns (if all observations are the same across sequential columns). In such a case, the corresponding optimal Lagrange multipliers are always zero, and we arrive at the same conclusion $\eta = 0$ from (S12) whether we include or exclude the corresponding columns in \mathbf{A} from $\mathbf{A}_{0,i}$.
- We do not have constant values in a column \mathbf{Y}_j , but the value of $\boldsymbol{\lambda}$ is such that the weighted mean(s) of the observations makes some constraints exactly met. As stated above, when tracing out a countably long sequence $\{\boldsymbol{\lambda}^{(0)}, \boldsymbol{\lambda}^{(1)}, \dots\}$ during gradient descent, it is almost sure that $\frac{\partial}{\partial \lambda_k^{(t)}} \mathbb{P}_{\mathbf{A}_{0,i}}(\boldsymbol{\lambda}^{(t)}) = 0$ for all i, k , and t .

Given these observations, we treat $\mathbb{P}_{\mathbf{A}_{0,i}}(\boldsymbol{\lambda})$ as locally constant with respect to $\boldsymbol{\lambda}$ in deriving the Hessian $\nabla^2 f(\boldsymbol{\lambda})$. The Hessian can be found element-wise

$$\begin{aligned} \frac{\partial^2}{\partial \lambda_h \partial \lambda_k} f(\boldsymbol{\lambda}) &= \frac{\partial}{\partial \lambda_h} \mathbf{N}_{k,k} = \tilde{\mathbf{X}}_k^\top \left[\left(\frac{\partial}{\partial \lambda_h} \mathbf{G} \right) \left\{ \sum_{i=1}^n \mathbf{e}_i \mathbf{e}_i^\top (\hat{\mathbf{Y}} - \mathbf{Y})(\mathbf{I}_m - \mathbb{P}_{\mathbf{A}_{0,i}}) \right\} \mathbf{Y}^\top \mathbf{G} + \right. \\ &\quad \mathbf{G} \left\{ \sum_{i=1}^n \mathbf{e}_i \mathbf{e}_i^\top \left(\frac{\partial}{\partial \lambda_h} \hat{\mathbf{Y}} \right) (\mathbf{I}_m - \mathbb{P}_{\mathbf{A}_{0,i}}) \right\} \mathbf{Y}^\top \mathbf{G} + \\ &\quad \left. \mathbf{G} \left\{ \sum_{i=1}^n \mathbf{e}_i \mathbf{e}_i^\top (\hat{\mathbf{Y}} - \mathbf{Y})(\mathbf{I}_m - \mathbb{P}_{\mathbf{A}_{0,i}}) \right\} \mathbf{Y}^\top \left(\frac{\partial}{\partial \lambda_h} \mathbf{G} \right) \right] \tilde{\mathbf{X}}_k \\ &= \tilde{\mathbf{X}}_k^\top \left[-\mathbf{G} \tilde{\mathbf{X}}_h \tilde{\mathbf{X}}_h^\top \mathbf{G} \left\{ \sum_{i=1}^n \mathbf{e}_i \mathbf{e}_i^\top (\hat{\mathbf{Y}} - \mathbf{Y})(\mathbf{I}_m - \mathbb{P}_{\mathbf{A}_{0,i}}) \right\} \mathbf{Y}^\top \mathbf{G} + \right. \\ &\quad \mathbf{G} \left\{ \sum_{i=1}^n \mathbf{e}_i \mathbf{e}_i^\top \mathbf{G} \tilde{\mathbf{X}}_h \tilde{\mathbf{X}}_h^\top \mathbf{G} \mathbf{Y} (\mathbf{I}_m - \mathbb{P}_{\mathbf{A}_{0,i}}) \right\} \mathbf{Y}^\top \mathbf{G} - \\ &\quad \left. \mathbf{G} \left\{ \sum_{i=1}^n \mathbf{e}_i \mathbf{e}_i^\top (\hat{\mathbf{Y}} - \mathbf{Y})(\mathbf{I}_m - \mathbb{P}_{\mathbf{A}_{0,i}}) \right\} \mathbf{Y}^\top \mathbf{G} \tilde{\mathbf{X}}_h \tilde{\mathbf{X}}_h^\top \mathbf{G} \right] \tilde{\mathbf{X}}_k, \end{aligned}$$

where we used (S11) for the gradient of \mathbf{G} and $\hat{\mathbf{Y}}$.

The first and third terms are transposes and contain \mathbf{N} (or \mathbf{N}^\top), and can be combined

$$\begin{aligned} \frac{\partial^2}{\partial \lambda_h \partial \lambda_k} f(\boldsymbol{\lambda}) = & \left[\sum_{i=1}^n (\tilde{\mathbf{X}}^\top \mathbf{G} \mathbf{e}_i \mathbf{e}_i^\top \mathbf{G} \tilde{\mathbf{X}}) \circ \left\{ \tilde{\mathbf{X}}^\top \mathbf{G} \mathbf{Y} (\mathbf{I}_m - \mathbb{P}_{\mathbf{A}_{0,i}}) \mathbf{Y}^\top \mathbf{G} \tilde{\mathbf{X}} \right\} \right]_{k,h} - \\ & \left[(\tilde{\mathbf{X}}^\top \mathbf{G} \tilde{\mathbf{X}}) \circ (\mathbf{N} + \mathbf{N}^\top) \right]_{k,h}. \end{aligned} \quad (\text{S17})$$

Finally, the Hessian of (S4) is

$$\begin{aligned} \nabla^2 f(\boldsymbol{\lambda}) = & (\tilde{\mathbf{X}}^\top \mathbf{G}^2 \tilde{\mathbf{X}}) \circ (\tilde{\mathbf{X}}^\top \mathbf{G} \mathbf{Y} \mathbf{Y}^\top \mathbf{G} \tilde{\mathbf{X}}) - (\tilde{\mathbf{X}}^\top \mathbf{G} \tilde{\mathbf{X}}) \circ (\mathbf{N} + \mathbf{N}^\top) - \\ & \sum_{i=1}^n (\tilde{\mathbf{X}}^\top \mathbf{G} \mathbf{e}_i \mathbf{e}_i^\top \mathbf{G} \tilde{\mathbf{X}}) \circ (\tilde{\mathbf{X}}^\top \mathbf{G} \mathbf{Y} \mathbb{P}_{\mathbf{A}_{0,i}} \mathbf{Y}^\top \mathbf{G} \tilde{\mathbf{X}}). \end{aligned} \quad \square$$

Proof of Proposition 4.2

For $\boldsymbol{\lambda} = \mathcal{F}(\boldsymbol{\gamma}) := \boldsymbol{\gamma} \circ \boldsymbol{\gamma}$, we have $g(\boldsymbol{\gamma}) = (f \circ \mathcal{F})(\boldsymbol{\gamma}) = f(\boldsymbol{\lambda})$. From Lemma S.1

$$\frac{\partial}{\partial \gamma_k} g(\boldsymbol{\gamma}) = \frac{\partial}{\partial \gamma_k} (f \circ \mathcal{F})(\boldsymbol{\gamma}) = 2\gamma_k \cdot \frac{\partial}{\partial \lambda_k} f(\boldsymbol{\lambda}),$$

where the right term is given by Proposition 4.1. Then the full gradient is

$$\nabla g(\boldsymbol{\gamma}) = 2\boldsymbol{\gamma} \circ \nabla f(\boldsymbol{\lambda}),$$

as desired. The Hessian $\nabla^2 g(\boldsymbol{\gamma})$ is element-wise

$$\begin{aligned} \frac{\partial^2}{\partial \gamma_h \partial \gamma_k} g(\boldsymbol{\gamma}) = & \frac{\partial}{\partial \gamma_h} \left\{ 2\gamma_k \cdot \frac{\partial}{\partial \lambda_k} f(\boldsymbol{\lambda}) \right\} \\ = & 2 \frac{\partial}{\partial \lambda_k} f(\boldsymbol{\lambda}) \mathbb{1}(k = h) + 2\gamma_k \cdot \frac{\partial}{\partial \gamma_h} \left\{ \frac{\partial}{\partial \lambda_k} f(\boldsymbol{\lambda}) \right\} \\ = & 2 \frac{\partial}{\partial \lambda_k} f(\boldsymbol{\lambda}) \mathbb{1}(k = h) + 4\gamma_k \gamma_h \cdot \frac{\partial^2}{\partial \lambda_h \partial \lambda_k} f(\boldsymbol{\lambda}), \end{aligned}$$

where the right term is given by Proposition 4.1. Then the full Hessian is

$$\nabla^2 g(\boldsymbol{\gamma}) = 2\mathbf{D}_{\nabla f(\boldsymbol{\lambda})} + 4(\boldsymbol{\gamma} \boldsymbol{\gamma}^\top) \circ \nabla^2 f(\boldsymbol{\lambda}). \quad \square$$

Proof of Proposition 4.3

Fix $\boldsymbol{\gamma} \in \mathcal{S}_{\sqrt{\tau}}$. The gradient $\nabla g(\boldsymbol{\gamma})$ has an orthogonal decomposition into a component in the tangent space of $\mathcal{S}_{\boldsymbol{\gamma}}$ (i.e. perpendicular to $\boldsymbol{\gamma}$) and a component normal to it (i.e. parallel to $\boldsymbol{\gamma}$)

$$\nabla g(\boldsymbol{\gamma}) = (\mathbf{I}_p - \mathbb{P}_{\boldsymbol{\gamma}}) \nabla g(\boldsymbol{\gamma}) + \mathbb{P}_{\boldsymbol{\gamma}} \nabla g(\boldsymbol{\gamma})$$

Suppose $\nabla_t g(\boldsymbol{\gamma}) \neq \mathbf{0}_p$, and let $\mathbf{v} := -(\mathbf{I}_p - \mathbb{P}_{\boldsymbol{\gamma}}) \nabla g(\boldsymbol{\gamma})$. Let $\{(\sqrt{\tau}, \theta) : \theta \in [0, 2\pi)\}$ be the radius-angle polar coordinate system which parameterizes the unique great circle in $\mathcal{S}_{\sqrt{\tau}}$ that contains $\boldsymbol{\gamma}$ and is coplanar with $\nabla_t g(\boldsymbol{\gamma})$. Without loss of generality, for $\theta \geq 0$ we use $\mathbf{R}_\theta \boldsymbol{\gamma}$ to represent rotations of $\boldsymbol{\gamma}$ around this circle in the

direction of \mathbf{v} , with \mathbf{R}_θ given by (S1). Observe

$$\mathbf{R}_\theta \boldsymbol{\gamma} = \|\boldsymbol{\gamma}\|_2 \mathbf{R}_\theta \underline{\boldsymbol{\gamma}} = \|\boldsymbol{\gamma}\|_2 \{(\cos \theta) \underline{\boldsymbol{\gamma}} + (\sin \theta) \underline{\mathbf{v}}\}. \quad (\text{S18})$$

Define the composite function $g_*(\theta) := (g \circ \mathbf{R}_\theta)(\boldsymbol{\gamma})$. The first total derivative of $g_*(\theta)$ with respect to θ is given by

$$\begin{aligned} \frac{d}{d\theta} g_*(\theta) &= \frac{d}{d\theta} (g \circ \mathbf{R}_\theta)(\boldsymbol{\gamma}) \\ &= \langle \nabla g(\boldsymbol{\gamma}), \frac{\partial}{\partial \theta} \mathbf{R}_\theta \boldsymbol{\gamma} \rangle \\ &= \langle \mathbb{P}_{\boldsymbol{\gamma}} \nabla g(\boldsymbol{\gamma}) - \|\mathbf{v}\|_2 \underline{\mathbf{v}}, \|\boldsymbol{\gamma}\|_2 \{(\cos \theta) \underline{\mathbf{v}} - (\sin \theta) \underline{\boldsymbol{\gamma}}\} \rangle \\ &= \|\boldsymbol{\gamma}\|_2 [(\cos \theta) \{\nabla g(\boldsymbol{\gamma})\}^\top \mathbb{P}_{\boldsymbol{\gamma}} \underline{\mathbf{v}} - (\sin \theta) \{\nabla g(\boldsymbol{\gamma})\}^\top \mathbb{P}_{\boldsymbol{\gamma}} \underline{\boldsymbol{\gamma}} - \\ &\quad (\cos \theta) \|\mathbf{v}\|_2 \underline{\mathbf{v}}^\top \underline{\mathbf{v}} + (\sin \theta) \|\mathbf{v}\|_2 \underline{\mathbf{v}}^\top \underline{\boldsymbol{\gamma}}] \\ &= \|\boldsymbol{\gamma}\|_2 [0 - (\sin \theta) \{\nabla g(\boldsymbol{\gamma})\}^\top \underline{\boldsymbol{\gamma}} - (\cos \theta) \|\mathbf{v}\|_2 + 0] \\ &= -(\sin \theta) \|\boldsymbol{\gamma}\|_2 \{\nabla g(\boldsymbol{\gamma})\}^\top \underline{\boldsymbol{\gamma}} - (\cos \theta) \|\boldsymbol{\gamma}\|_2 \|\mathbf{v}\|_2. \end{aligned}$$

Evaluated at $\theta = 0$, we obtain

$$\frac{d}{d\theta} g_*(0) = -\|\boldsymbol{\gamma}\|_2 \|\mathbf{v}\|_2,$$

as desired. The second total derivative of $g_*(\theta)$ with respect to θ is given by

$$\begin{aligned} \frac{d^2}{d\theta^2} g_*(\theta) &= \frac{d^2}{d\theta^2} (g \circ \mathbf{R}_\theta)(\boldsymbol{\gamma}) \\ &= \langle \nabla \frac{d}{d\theta} g_*(\theta), \|\boldsymbol{\gamma}\|_2 \{(\cos \theta) \underline{\mathbf{v}} - (\sin \theta) \underline{\boldsymbol{\gamma}}\} \rangle \\ &= -\|\boldsymbol{\gamma}\|_2 \langle \nabla [(\sin \theta) \{\nabla g(\boldsymbol{\gamma})\}^\top \underline{\boldsymbol{\gamma}} + (\cos \theta) \|\boldsymbol{\gamma}\|_2 \|\mathbf{v}\|_2], (\cos \theta) \underline{\mathbf{v}} - (\sin \theta) \underline{\boldsymbol{\gamma}} \rangle \\ &= -(\cos^2 \theta) \|\boldsymbol{\gamma}\|_2 \underline{\mathbf{v}}^\top \nabla (\|\boldsymbol{\gamma}\|_2 \|\mathbf{v}\|_2) + (\sin \theta \text{ terms}). \end{aligned} \quad (\text{S19})$$

Our goal is to evaluate this expression at $\theta = 0$, so each term involving $\sin \theta$ will be zero. As such, we focus on only the first term, especially the gradient (which is with respect to $\boldsymbol{\gamma}$). As a preliminary matter, we evaluate $\nabla \underline{\boldsymbol{\gamma}}$

$$\begin{aligned} \frac{\partial}{\partial \gamma_h} \frac{\gamma_k}{\|\boldsymbol{\gamma}\|_2} &= \frac{\mathbb{1}(k=h) \|\boldsymbol{\gamma}\|_2 - \gamma_k \frac{1}{2\|\boldsymbol{\gamma}\|_2} 2\gamma_h}{\|\boldsymbol{\gamma}\|_2^2}, \\ \Rightarrow \quad \nabla \underline{\boldsymbol{\gamma}} &= \frac{1}{\|\boldsymbol{\gamma}\|_2} (\mathbf{I}_p - \underline{\boldsymbol{\gamma}} \underline{\boldsymbol{\gamma}}^\top). \end{aligned}$$

The gradient in (S19) involves solving both $\nabla \|\boldsymbol{\gamma}\|_2$ and $\nabla \|\mathbf{v}\|_2$. The first is

$$\nabla \|\boldsymbol{\gamma}\|_2 = \nabla (\boldsymbol{\gamma}^\top \boldsymbol{\gamma})^{1/2} = \frac{1}{2\|\boldsymbol{\gamma}\|_2} \nabla \boldsymbol{\gamma}^\top \boldsymbol{\gamma} = \underline{\boldsymbol{\gamma}}. \quad (\text{S20})$$

Next, since $\|\mathbf{v}\|_2 = [\{\nabla g(\boldsymbol{\gamma})\}^\top (\mathbf{I}_p - \mathbb{P}_{\boldsymbol{\gamma}}) \{\nabla g(\boldsymbol{\gamma})\}]^{1/2} = [\{\nabla g(\boldsymbol{\gamma})\}^\top \nabla g(\boldsymbol{\gamma}) - \{\underline{\boldsymbol{\gamma}}^\top \nabla g(\boldsymbol{\gamma})\}^2]^{1/2}$

$$\begin{aligned}
\nabla \|\mathbf{v}\|_2 &= \nabla [\{\nabla g(\boldsymbol{\gamma})\}^\top \nabla g(\boldsymbol{\gamma}) - \{\underline{\boldsymbol{\gamma}}^\top \nabla g(\boldsymbol{\gamma})\}^2]^{1/2} \\
&= \frac{1}{2\|\mathbf{v}\|_2} \left[2\{\nabla^2 g(\boldsymbol{\gamma})\} \nabla g(\boldsymbol{\gamma}) - 2\underline{\boldsymbol{\gamma}}^\top \nabla g(\boldsymbol{\gamma}) \left\{ \frac{1}{\|\boldsymbol{\gamma}\|_2} (\mathbf{I}_p - \underline{\boldsymbol{\gamma}} \underline{\boldsymbol{\gamma}}^\top) \nabla g(\boldsymbol{\gamma}) + \{\nabla^2 g(\boldsymbol{\gamma})\} \underline{\boldsymbol{\gamma}} \right\} \right] \\
&= \frac{1}{\|\mathbf{v}\|_2} \left[\{\nabla^2 g(\boldsymbol{\gamma})\} \nabla g(\boldsymbol{\gamma}) + \underline{\boldsymbol{\gamma}}^\top \nabla g(\boldsymbol{\gamma}) \left\{ \frac{\mathbf{v}}{\|\boldsymbol{\gamma}\|_2} - \{\nabla^2 g(\boldsymbol{\gamma})\} \underline{\boldsymbol{\gamma}} \right\} \right] \\
&= \frac{1}{\|\mathbf{v}\|_2} \left[\mathbf{v} \cdot \frac{\underline{\boldsymbol{\gamma}}^\top \nabla g(\boldsymbol{\gamma})}{\|\boldsymbol{\gamma}\|_2} + \{\nabla^2 g(\boldsymbol{\gamma})\} (\mathbf{I}_p - \underline{\boldsymbol{\gamma}} \underline{\boldsymbol{\gamma}}^\top) \nabla g(\boldsymbol{\gamma}) \right] \\
&= \underline{\mathbf{v}} \cdot \frac{\underline{\boldsymbol{\gamma}}^\top \nabla g(\boldsymbol{\gamma})}{\|\boldsymbol{\gamma}\|_2} - \{\nabla^2 g(\boldsymbol{\gamma})\} \underline{\mathbf{v}}. \tag{S21}
\end{aligned}$$

Combining (S20) and (S21), we complete (S19)

$$\begin{aligned}
\frac{d^2}{d\theta^2} g_*(\theta) &= -(\cos^2 \theta) \|\boldsymbol{\gamma}\|_2 \underline{\mathbf{v}}^\top \{ \|\boldsymbol{\gamma}\|_2 \nabla \|\mathbf{v}\|_2 + \|\mathbf{v}\|_2 \nabla \|\boldsymbol{\gamma}\|_2 \} + (\sin \theta \text{ terms}) \\
&= -(\cos^2 \theta) \|\boldsymbol{\gamma}\|_2 \left[\|\boldsymbol{\gamma}\|_2 \frac{\underline{\boldsymbol{\gamma}}^\top \nabla g(\boldsymbol{\gamma})}{\|\boldsymbol{\gamma}\|_2} - \|\boldsymbol{\gamma}\|_2 \underline{\mathbf{v}}^\top \{\nabla^2 g(\boldsymbol{\gamma})\} \underline{\mathbf{v}} + \|\mathbf{v}\|_2 \cdot 0 \right] + (\sin \theta \text{ terms}) \\
&= (\cos^2 \theta) \left[\|\boldsymbol{\gamma}\|_2^2 \underline{\mathbf{v}}^\top \{\nabla^2 g(\boldsymbol{\gamma})\} \underline{\mathbf{v}} - \boldsymbol{\gamma}^\top \nabla g(\boldsymbol{\gamma}) \right] + (\sin \theta \text{ terms}).
\end{aligned}$$

Finally, evaluated at $\theta = 0$, the second total derivative of $g_*(\theta)$ is

$$\frac{d^2}{d\theta^2} g_*(0) = \tau \cdot \underline{\mathbf{v}}^\top \{\nabla^2 g(\boldsymbol{\gamma})\} \underline{\mathbf{v}} - \boldsymbol{\gamma}^\top \nabla g(\boldsymbol{\gamma}),$$

as desired. □

S3 Fast Embedded Problem Solving

Recall the embedded quantile estimation problem consists of solving

$$\hat{\mathbf{Q}} := \arg \min_{\mathbf{Q} \in \mathbb{R}^{n \times m}} \|\mathbf{Q} - \hat{\mathbf{Y}}\|_F^2, \quad \text{subject to} \quad \mathbf{B} - \mathbf{Q}\mathbf{A} \leq \mathbf{0}_{n \times m}, \quad (\text{S22})$$

where $\hat{\mathbf{Y}}$ is given by (6). The matrices $\mathbf{A} \in \mathbb{R}^{m \times (m+1)}$ and $\mathbf{B} \in \mathbb{R}^{n \times (m+1)}$ impose monotonicity constraints and box constraints $b_L \leq q_{i,j} \leq b_U$ for all i, j . We require $b_L < b_U$, but we permit both $b_L = -\infty$ and $b_U = \infty$. \mathbf{A} and \mathbf{B} respectively take form

$$\mathbf{A} = \begin{bmatrix} +1 & -1 & 0 & 0 & \cdots & 0 & 0 \\ 0 & +1 & -1 & 0 & \cdots & 0 & 0 \\ 0 & 0 & +1 & -1 & \cdots & 0 & 0 \\ 0 & 0 & 0 & +1 & \cdots & 0 & 0 \\ \vdots & \vdots & \vdots & \vdots & \ddots & \vdots & \vdots \\ 0 & 0 & 0 & 0 & \cdots & +1 & -1 \end{bmatrix}, \quad (\text{S23})$$

$$\mathbf{B} = [b_L \mathbf{1}_n \quad \mathbf{0}_{n \times (m-1)} \quad -b_U \mathbf{1}_n]. \quad (\text{S24})$$

The Lagrangian of the embedded optimization problem is

$$\mathcal{L}(\mathbf{Q}, \mathbf{H}) = \frac{1}{2} \|\mathbf{Q} - \hat{\mathbf{Y}}\|_F^2 + \text{tr} \{ (\mathbf{B} - \mathbf{Q}\mathbf{A})^\top \mathbf{H} \}, \quad (\text{S25})$$

where $\mathbf{H} \in \mathbb{R}^{n \times (m+1)} \geq \mathbf{0}_{n \times (m+1)}$ is the associated Lagrange multiplier. Optimality is given by the stability and primal feasibility KKT conditions

$$\begin{aligned} \frac{\partial}{\partial \mathbf{Q}} \mathcal{L}(\hat{\mathbf{Q}}, \hat{\mathbf{H}}) &= \mathbf{0}_{n \times m}, \\ \mathbf{B} - \hat{\mathbf{Q}}\mathbf{A} &= \mathbf{0}_{n \times (m+1)}, \end{aligned}$$

where the second condition is equivalent to $\frac{\partial}{\partial \mathbf{H}} \mathcal{L}(\hat{\mathbf{Q}}, \hat{\mathbf{H}}) = \mathbf{0}_{n \times (m+1)}$; the solution pair $\hat{\mathbf{Q}}, \hat{\mathbf{H}}$ form a saddle point in (\mathbf{Q}, \mathbf{H}) space. The derivative of $\mathcal{L}(\mathbf{Q}, \mathbf{H})$ with respect to \mathbf{Q} is $\frac{\partial}{\partial \mathbf{Q}} \mathcal{L}(\mathbf{Q}, \mathbf{H}) = \mathbf{Q} - \hat{\mathbf{Y}} - \mathbf{H}\mathbf{A}^\top$, and hence $\hat{\mathbf{Q}} = \hat{\mathbf{Y}} + \hat{\mathbf{H}}\mathbf{A}^\top$. This allows us to perform projected gradient ascent on \mathbf{H} alone, where the projection step is onto the positive part of \mathbf{H} , to obey $\mathbf{H} \geq \mathbf{0}$. Given t^{th} iterate $\mathbf{H}^{(t)}$ and dampening parameter $\alpha > 0$, we substitute $\mathbf{Q}^{(t)} = \hat{\mathbf{Y}} + \mathbf{H}^{(t)}\mathbf{A}^\top$ and write the ascent step

$$\begin{aligned} \mathbf{H}^{(t+1)} &= \left\{ \mathbf{H}^{(t)} + \alpha \cdot \frac{\partial}{\partial \mathbf{H}} \mathcal{L}(\mathbf{Q}^{(t)}, \mathbf{H}^{(t)}) \right\}_+ \\ &= \left\{ \mathbf{H}^{(t)} + \alpha (\mathbf{B} - \mathbf{Q}^{(t)}\mathbf{A}) \right\}_+ \\ &= \left\{ \mathbf{H}^{(t)} + \alpha (\mathbf{B} - \hat{\mathbf{Y}}\mathbf{A} - \mathbf{H}^{(t)}\mathbf{A}^\top\mathbf{A}) \right\}_+ \\ &= \left\{ \alpha (\mathbf{B} - \hat{\mathbf{Y}}\mathbf{A}) + \alpha \mathbf{H}^{(t)} (\alpha^{-1} \mathbf{I}_{m+1} - \mathbf{A}^\top\mathbf{A}) \right\}_+. \end{aligned} \quad (\text{S26})$$

We take $\alpha = 1/2$, so that each gradient iteration involves evaluating $\mathbf{H}^{(t)}(2\mathbf{I}_{m+1} - \mathbf{A}^\top \mathbf{A})$. The form of \mathbf{A} from (S23) admits

$$2\mathbf{I}_{m+1} - \mathbf{A}^\top \mathbf{A} = \begin{bmatrix} 1 & 1 & 0 & 0 & \cdots & 0 & 0 \\ 1 & 0 & 1 & 0 & \cdots & 0 & 0 \\ 0 & 1 & 0 & 1 & \cdots & 0 & 0 \\ 0 & 0 & 1 & 0 & \cdots & 0 & 0 \\ \vdots & \vdots & \vdots & \vdots & \ddots & \vdots & \vdots \\ 0 & 0 & 0 & 0 & \cdots & 0 & 1 \\ 0 & 0 & 0 & 0 & \cdots & 1 & 1 \end{bmatrix},$$

so that right-multiplication of $\mathbf{H}^{(t)}$ by $2\mathbf{I}_{m+1} - \mathbf{A}^\top \mathbf{A}$ is simply a summation operation over columns of $\mathbf{H}^{(t)}$. Specifically, this is

$$\mathbf{H}^{(t)}(2\mathbf{I}_{m+1} - \mathbf{A}^\top \mathbf{A}) = [\mathbf{H}_{2:(m+1)}^{(t)} \quad \mathbf{H}_{m+1}^{(t)}] + [\mathbf{H}_1^{(t)} \quad \mathbf{H}_{1:m}^{(t)}], \quad (\text{S27})$$

where $\mathbf{H}_{i:j} := [\mathbf{H}_i \quad \mathbf{H}_{i+1} \quad \cdots \quad \mathbf{H}_j]$. Defining $\mathbf{C}_{\hat{\mathbf{Y}}} := \mathbf{B} - \hat{\mathbf{Y}}\mathbf{A}$ and plugging (S27) into (S26), we have a final gradient step of

$$\mathbf{H}^{(t+1)} = \left\{ \frac{1}{2} \left(\mathbf{C}_{\hat{\mathbf{Y}}} + [\mathbf{H}_{2:(m+1)}^{(t)} \quad \mathbf{H}_{m+1}^{(t)}] + [\mathbf{H}_1^{(t)} \quad \mathbf{H}_{1:m}^{(t)}] \right) \right\}_+, \quad (\text{S28})$$

which is simultaneous across all i and which does not involve vector or matrix multiplication. Importantly too, equation (S28) updates rows of $\mathbf{H}^{(t)}$ independently of each other, and if a row $\hat{\mathbf{y}}_i$ of $\hat{\mathbf{Y}}$ does not violate any constraints in $\mathbf{B} - \hat{\mathbf{Y}}\mathbf{A} \leq \mathbf{0}$, the corresponding row $\boldsymbol{\eta}_i$ of $\hat{\mathbf{H}}$ will be $\mathbf{0}_{m+1}$. As such, gradient ascent S28 may be focused on those rows $\boldsymbol{\eta}_i$ where $\mathbf{b} - \mathbf{A}^\top \hat{\mathbf{y}}_i \leq \mathbf{0}_{m+1}$ is violated.

S4 Specific Implementation of Geodesic Descent

In the $p \gg n$ case or the $n \gg p$ case, efficient implementation should avoid handling matrices of size $p \times p$ or $n \times n$, respectively. Here we algebraically manipulate the matrix operations to “fold in” the larger dimension, leaving most matrix operations to occur between objects of the smaller dimension.

To begin, note the matrix product $\mathbf{G}\tilde{\mathbf{X}}$ can be rearranged with the push-through identity:

$$\begin{aligned}\mathbf{G}\tilde{\mathbf{X}} &= (\tilde{\mathbf{X}}\mathbf{D}_\gamma^2\tilde{\mathbf{X}}^\top + \mathbf{I}_n)^{-1}\tilde{\mathbf{X}} \\ &= \tilde{\mathbf{X}}(\mathbf{D}_\gamma^2\tilde{\mathbf{X}}^\top\tilde{\mathbf{X}} + \mathbf{I}_p)^{-1} \\ &=: \tilde{\mathbf{X}}\mathbf{F},\end{aligned}\tag{S29}$$

where $\mathbf{F} := (\mathbf{D}_\gamma^2\tilde{\mathbf{X}}^\top\tilde{\mathbf{X}} + \mathbf{I}_p)^{-1}$ has been defined for convenience. Since $\mathbf{G} \in \mathbb{R}^{n \times n}$ and $\mathbf{F} \in \mathbb{R}^{p \times p}$, the identity $\mathbf{G}\tilde{\mathbf{X}} = \tilde{\mathbf{X}}\mathbf{F}$ will be helpful in reducing object sizes when n and p are different in scale.

S4.1 Gradient $\nabla f(\boldsymbol{\lambda})$

The gradient $\nabla f(\boldsymbol{\lambda})$ information is contained in the diagonal entries of \mathbf{N} , which again are

$$\frac{\partial}{\partial \lambda_k} f(\boldsymbol{\lambda}) = \tilde{\mathbf{X}}_k^\top \mathbf{G} \left\{ \sum_{i=1}^n \mathbf{e}_i \mathbf{e}_i^\top (\hat{\mathbf{Y}} - \mathbf{Y})(\mathbf{I}_m - \mathbb{P}_{\mathbf{A}_{0,i}}) \right\} \mathbf{Y}^\top \mathbf{G} \tilde{\mathbf{X}}_k \tag{S30}$$

Let $\tilde{\mathbf{E}} \in \mathbb{R}^{n \times m}$ be the matrix inside the braces in (S30), formed by row-wise modifying $\hat{\mathbf{E}} = \hat{\mathbf{Y}} - \mathbf{Y}$ through right-multiplication with $\mathbf{I}_m - \mathbb{P}_{\mathbf{A}_{0,i}}$. Note $\tilde{\mathbf{E}} = \sum_{i=1}^n \mathbf{e}_i \mathbf{e}_i^\top \hat{\mathbf{E}}$. Equation (S30) can be rewritten:

$$\begin{aligned}\frac{\partial}{\partial \lambda_k} f(\boldsymbol{\lambda}) &= \sum_{i=1}^n \tilde{\mathbf{X}}_k^\top \mathbf{G} \mathbf{Y} \tilde{\mathbf{E}}^\top \mathbf{e}_i \cdot \tilde{\mathbf{X}}_k^\top \mathbf{G} \mathbf{e}_i, \quad \text{hence} \\ \nabla f(\boldsymbol{\lambda}) &= \sum_{i=1}^n (\tilde{\mathbf{X}}^\top \mathbf{G} \mathbf{Y} \tilde{\mathbf{E}}^\top \mathbf{e}_i) \circ (\tilde{\mathbf{X}}^\top \mathbf{G} \mathbf{e}_i) \\ &= \left\{ (\tilde{\mathbf{X}}^\top \mathbf{G} \mathbf{Y} \tilde{\mathbf{E}}^\top) \circ (\tilde{\mathbf{X}}^\top \mathbf{G}) \right\} \mathbf{1}_n.\end{aligned}$$

Since $\mathbf{G} \in \mathbb{R}^{n \times n}$, this form is suitable when $p \gg n$, otherwise we use the identity in (S29)

$$\nabla f(\boldsymbol{\lambda}) = \left\{ (\mathbf{F}^\top \tilde{\mathbf{X}}^\top \mathbf{Y} \tilde{\mathbf{E}}^\top) \circ (\mathbf{F}^\top \tilde{\mathbf{X}}^\top) \right\} \mathbf{1}_n, \tag{S31}$$

where $\mathbf{F} \in \mathbb{R}^{p \times p}$. The matrix $\tilde{\mathbf{X}}^\top \mathbf{Y} \in \mathbb{R}^{p \times m}$ can be calculated once and stored in memory.

S4.2 2nd Derivative $g''_*(0)$

The geodesic step involves evaluating second derivative, which can be written

$$g''_*(0) = \tau \cdot \mathbf{v}^\top \{ \nabla^2 g(\gamma) \} \mathbf{v} - \gamma^\top \nabla g(\gamma).$$

Letting $\boldsymbol{\lambda} = \mathcal{F}(\gamma) = \gamma \circ \gamma$, the Hessian $\nabla^2 g(\gamma)$ is

$$\nabla^2 g(\gamma) = 2\mathbf{D}_{\nabla f(\boldsymbol{\lambda})} + 4(\gamma\gamma^\top) \circ \nabla^2 f(\boldsymbol{\lambda}),$$

which we do not want to directly calculate when $p \gg n$. Instead, we can express the corresponding component of the second derivative as a sum of terms

$$\tau \cdot \underline{\mathbf{v}}^\top \{ \nabla^2 g(\boldsymbol{\gamma}) \} \underline{\mathbf{v}} = 2\tau \cdot \{ \underline{\mathbf{v}} \circ \underline{\mathbf{v}} \circ \nabla f(\boldsymbol{\lambda}) \} \mathbf{1}_p + 4\tau^2 \cdot (\underline{\mathbf{v}} \circ \underline{\boldsymbol{\gamma}})^\top \{ \nabla^2 f(\boldsymbol{\lambda}) \} (\underline{\mathbf{v}} \circ \underline{\boldsymbol{\gamma}}). \quad (\text{S32})$$

For the second term of (S32), we combine the Hessian terms from Proposition 2 into a single summation over $i \in [n]$

$$\begin{aligned} \nabla^2 f(\boldsymbol{\lambda}) = \sum_{i=1}^n & \left[\left\{ \tilde{\mathbf{X}}^\top \mathbf{G} \underline{\mathbf{e}}_i \underline{\mathbf{e}}_i^\top \mathbf{G} \tilde{\mathbf{X}} \right\} \circ \left\{ \tilde{\mathbf{X}}^\top \mathbf{G} \mathbf{Y} (\mathbf{I}_m - \mathbb{P}_{\mathbf{A}_{0,i}}) \mathbf{Y}^\top \mathbf{G} \tilde{\mathbf{X}} \right\} - \right. \\ & \left. \left\{ \tilde{\mathbf{X}}^\top \mathbf{G} \tilde{\mathbf{X}} \right\} \circ \left\{ \tilde{\mathbf{X}}^\top \mathbf{G} (\mathbf{Y} \tilde{\mathbf{E}}^\top \underline{\mathbf{e}}_i \underline{\mathbf{e}}_i^\top + \underline{\mathbf{e}}_i \underline{\mathbf{e}}_i^\top \tilde{\mathbf{E}} \mathbf{Y}^\top) \mathbf{G} \tilde{\mathbf{X}} \right\} \right], \end{aligned}$$

so that now

$$\begin{aligned} (\underline{\mathbf{v}} \circ \underline{\boldsymbol{\gamma}})^\top \{ \nabla^2 f(\boldsymbol{\lambda}) \} (\underline{\mathbf{v}} \circ \underline{\boldsymbol{\gamma}}) &= \sum_{k=1}^p \sum_{h=1}^p \gamma_k \gamma_h \underline{\mathbf{v}}_k \underline{\mathbf{v}}_h \sum_{i=1}^n \left[\tilde{\mathbf{X}}_k^\top \mathbf{G} \underline{\mathbf{e}}_i \underline{\mathbf{e}}_i^\top \mathbf{G} \tilde{\mathbf{X}}_h \tilde{\mathbf{X}}_k^\top \mathbf{G} \mathbf{Y} (\mathbf{I}_m - \mathbb{P}_{\mathbf{A}_{0,i}}) \mathbf{Y}^\top \mathbf{G} \tilde{\mathbf{X}}_h - \right. \\ & \quad \left. \tilde{\mathbf{X}}_k^\top \mathbf{G} \tilde{\mathbf{X}}_h \tilde{\mathbf{X}}_k^\top \mathbf{G} (\mathbf{Y} \tilde{\mathbf{E}}^\top \underline{\mathbf{e}}_i \underline{\mathbf{e}}_i^\top + \underline{\mathbf{e}}_i \underline{\mathbf{e}}_i^\top \tilde{\mathbf{E}} \mathbf{Y}^\top) \mathbf{G} \tilde{\mathbf{X}}_h \right] \\ &= \sum_{i=1}^n \sum_{k=1}^p \gamma_k \underline{\mathbf{v}}_k \sum_{h=1}^p \tilde{\mathbf{X}}_k^\top \mathbf{G} \underline{\mathbf{e}}_i \underline{\mathbf{e}}_i^\top \mathbf{G} \tilde{\mathbf{X}} (\gamma_h \underline{\mathbf{v}}_h \underline{\mathbf{e}}_h \underline{\mathbf{e}}_h^\top) \tilde{\mathbf{X}}^\top \mathbf{G} \mathbf{Y} (\mathbf{I}_m - \mathbb{P}_{\mathbf{A}_{0,i}}) \mathbf{Y}^\top \mathbf{G} \tilde{\mathbf{X}}_k - \\ & \quad \sum_{i=1}^n \sum_{k=1}^p \gamma_k \underline{\mathbf{v}}_k \sum_{h=1}^p \tilde{\mathbf{X}}_k^\top \mathbf{G} \tilde{\mathbf{X}} (\gamma_h \underline{\mathbf{v}}_h \underline{\mathbf{e}}_h \underline{\mathbf{e}}_h^\top) \tilde{\mathbf{X}}^\top \mathbf{G} (\mathbf{Y} \tilde{\mathbf{E}}^\top \underline{\mathbf{e}}_i \underline{\mathbf{e}}_i^\top + \underline{\mathbf{e}}_i \underline{\mathbf{e}}_i^\top \tilde{\mathbf{E}} \mathbf{Y}^\top) \mathbf{G} \tilde{\mathbf{X}}_k \\ &= \sum_{i=1}^n \sum_{k=1}^p \sum_{h=1}^p \underline{\mathbf{e}}_i^\top \mathbf{G} \tilde{\mathbf{X}} (\gamma_k \underline{\mathbf{v}}_k \underline{\mathbf{e}}_k \underline{\mathbf{e}}_k^\top) \tilde{\mathbf{X}}^\top \mathbf{G} \mathbf{Y} (\mathbf{I}_m - \mathbb{P}_{\mathbf{A}_{0,i}}) \mathbf{Y}^\top \mathbf{G} \tilde{\mathbf{X}} (\gamma_h \underline{\mathbf{v}}_h \underline{\mathbf{e}}_h \underline{\mathbf{e}}_h^\top) \tilde{\mathbf{X}}^\top \mathbf{G} \underline{\mathbf{e}}_i - \\ & \quad \sum_{i=1}^n \sum_{p=1}^p \sum_{h=1}^p \underline{\mathbf{e}}_i^\top \tilde{\mathbf{E}} \mathbf{Y}^\top \mathbf{G} \tilde{\mathbf{X}} (\gamma_h \underline{\mathbf{v}}_h \underline{\mathbf{e}}_h \underline{\mathbf{e}}_h^\top) \tilde{\mathbf{X}}^\top \mathbf{G} \tilde{\mathbf{X}} (\gamma_k \underline{\mathbf{v}}_k \underline{\mathbf{e}}_k \underline{\mathbf{e}}_k^\top) \tilde{\mathbf{X}}^\top \mathbf{G} \underline{\mathbf{e}}_i - \\ & \quad \sum_{i=1}^n \sum_{p=1}^p \sum_{h=1}^p \underline{\mathbf{e}}_i^\top \mathbf{G} \tilde{\mathbf{X}} (\gamma_h \underline{\mathbf{v}}_h \underline{\mathbf{e}}_h \underline{\mathbf{e}}_h^\top) \tilde{\mathbf{X}}^\top \mathbf{G} \tilde{\mathbf{X}} (\gamma_k \underline{\mathbf{v}}_k \underline{\mathbf{e}}_k \underline{\mathbf{e}}_k^\top) \tilde{\mathbf{X}}^\top \mathbf{G} \mathbf{Y} \tilde{\mathbf{E}}^\top \underline{\mathbf{e}}_i \\ &= \sum_{i=1}^n \underline{\mathbf{e}}_i^\top \mathbf{G} \tilde{\mathbf{X}} \mathbf{D}_{\underline{\boldsymbol{\gamma}} \circ \underline{\mathbf{v}}} \tilde{\mathbf{X}}^\top \mathbf{G} \mathbf{Y} (\mathbf{I}_m - \mathbb{P}_{\mathbf{A}_{0,i}}) \mathbf{Y}^\top \mathbf{G} \tilde{\mathbf{X}} \mathbf{D}_{\underline{\boldsymbol{\gamma}} \circ \underline{\mathbf{v}}} \tilde{\mathbf{X}}^\top \mathbf{G} \underline{\mathbf{e}}_i - \\ & \quad 2 \sum_{i=1}^n \underline{\mathbf{e}}_i^\top \tilde{\mathbf{E}} \mathbf{Y}^\top \mathbf{G} \tilde{\mathbf{X}} \mathbf{D}_{\underline{\boldsymbol{\gamma}} \circ \underline{\mathbf{v}}} \tilde{\mathbf{X}}^\top \mathbf{G} \tilde{\mathbf{X}} \mathbf{D}_{\underline{\boldsymbol{\gamma}} \circ \underline{\mathbf{v}}} \tilde{\mathbf{X}}^\top \mathbf{G} \underline{\mathbf{e}}_i. \end{aligned}$$

Then defining:

$$\begin{aligned} \mathbf{V} &:= \mathbf{Y}^\top \mathbf{G} \tilde{\mathbf{X}} \mathbf{D}_{\underline{\boldsymbol{\gamma}} \circ \underline{\mathbf{v}}} \tilde{\mathbf{X}}^\top \mathbf{G} &= \mathbf{Y}^\top \tilde{\mathbf{X}} \mathbf{F} \mathbf{D}_{\underline{\boldsymbol{\gamma}} \circ \underline{\mathbf{v}}} \mathbf{F}^\top \tilde{\mathbf{X}}^\top, \\ \mathbf{W} &:= \mathbf{Y}^\top \mathbf{G} \tilde{\mathbf{X}} \mathbf{D}_{\underline{\boldsymbol{\gamma}} \circ \underline{\mathbf{v}}} \tilde{\mathbf{X}}^\top \mathbf{G} \tilde{\mathbf{X}} \mathbf{D}_{\underline{\boldsymbol{\gamma}} \circ \underline{\mathbf{v}}} \tilde{\mathbf{X}}^\top \mathbf{G} &= \mathbf{Y}^\top \tilde{\mathbf{X}} \mathbf{F} \mathbf{D}_{\underline{\boldsymbol{\gamma}} \circ \underline{\mathbf{v}}} \mathbf{F}^\top \tilde{\mathbf{X}}^\top \tilde{\mathbf{X}} \mathbf{D}_{\underline{\boldsymbol{\gamma}} \circ \underline{\mathbf{v}}} \mathbf{F}^\top \tilde{\mathbf{X}}^\top, \end{aligned}$$

the second derivative is:

$$g''_*(0) = 2\tau \cdot \{ \underline{\mathbf{v}} \circ \underline{\mathbf{v}} \circ \nabla f(\boldsymbol{\lambda}) \} \mathbf{1}_p + 4\tau^2 \sum_{i=1}^n \mathbf{V}_i^\top (\mathbf{I}_m - \mathbb{P}_{\mathbf{A}_{0,i}}) \mathbf{V}_i - 16\tau^2 \langle \mathbf{W}, \tilde{\mathbf{E}}^\top \rangle_F - \boldsymbol{\gamma}^\top \nabla g(\boldsymbol{\gamma}). \quad (\text{S33})$$

Assuming $n, p > m$, the largest object which needs to be calculated and stored is $p \times n$ in size.

S5 Algorithms

Algorithm 1 recounts the modified coordinate descent algorithm as proposed by [Tucker et al. \(2023\)](#). Algorithm 2 describes our procedure for solving the embedded problem using the gradient methods discussed in Section S3. Algorithm 3 describes our proposed geodesic algorithm.

Algorithm 1: Modified Coordinate Descent (MCD)

Input: Total allowance $\tau > 0$; error tolerance parameters $\varepsilon_1 > 0$ and $\varepsilon_2 > 0$; constraint matrices $\mathbf{B} \in \mathbb{R}^{n \times (m+1)}$ and $\mathbf{A} \in \mathbb{R}^{m \times (m+1)}$; column-centered regressor matrix $\mathbf{X} \in \mathbb{R}^{n \times p}$; empirical quantile functions $\mathbf{Y} \in \mathbb{R}^{n \times m}$; initial allowance vector $\boldsymbol{\lambda}^{(0)}$; maximum iteration count $T \in \mathbb{N}_1$.

Output: Allowance vector $\hat{\boldsymbol{\lambda}}$ solving the FRiSO sparsity problem (7).

```

1 Initialize  $t \leftarrow 0$ .
2 Initialize error  $\leftarrow \varepsilon_1 + 1$ .
3 while error  $> \varepsilon_1$  and  $t < T$  do
4   Update  $t \leftarrow t + 1$ .
5   Set  $\boldsymbol{\lambda}^{(t)} \leftarrow \boldsymbol{\lambda}^{(t-1)}$ .
6   for  $k = 1, \dots, p$  do
7     if  $\sum_{k' \neq k} \lambda_{k'}^{(t)} > \varepsilon_2$  then
8       Define  $\mathbf{L}_k^{(t)}(\alpha) := \{\tilde{\boldsymbol{\lambda}}(\alpha) : 0 \leq \alpha \leq 1\} \subset \mathbf{T}$  as the line segment spanning  $\mathbf{T}$ , which connects
9        $\boldsymbol{\lambda}^{(t)}$  and the  $k^{\text{th}}$  corner of  $\mathbf{T}$  (given by  $\tau \cdot \mathbf{e}_k$ ), where  $\tilde{\lambda}_k(1) = \tau$  and  $\tilde{\lambda}_k(0) = 0$ .
10      Calculate:
          
$$\hat{\alpha} = \arg \min_{0 \leq \alpha \leq 1} \sum_{i=1}^n d_W^2(\mathbf{y}_i, \hat{\mathbf{q}}(\mathbf{x}_i; \tilde{\boldsymbol{\lambda}}(\alpha))).$$

          That is, perform a line search to minimize the FRiSO objective function along  $\mathbf{L}_k^{(t)}(\alpha)$ .
11      Update  $\boldsymbol{\lambda}^{(t)} \leftarrow \tilde{\boldsymbol{\lambda}}(\hat{\alpha})$ .
12   Update error  $\leftarrow \|\boldsymbol{\lambda}^{(t)} - \boldsymbol{\lambda}^{(t-1)}\|_\infty$ .
13 Set  $\hat{\boldsymbol{\lambda}} \leftarrow \boldsymbol{\lambda}^{(t)}$ .
```

Algorithm 2: Quantile Estimation (“Embedded”) Problem

Input: Error tolerance parameter $\varepsilon > 0$; constraint matrices $\mathbf{A} \in \mathbb{R}^{m \times (m+1)}$ and $\mathbf{B} \in \mathbb{R}^{m \times (m+1)}$ from (S23) and (S24), respectively; unconstrained predictor matrix $\hat{\mathbf{Y}}$ from (6); maximum iteration count $T \in \mathbb{N}_1$.

Output: Estimated quantile matrix $\hat{\mathbf{Q}}$ solving the embedded problem (8).

- 1 Define $\mathbf{C} := \mathbf{B} - \hat{\mathbf{Y}}\mathbf{A}$, and identify the index set $\mathcal{I} = \{i : \mathbf{c}_i \not\leq 0\}$ (i.e. the rows of \mathbf{C} which have at least one positive entry, indicating a violated constraint).
- 2 **if** $\mathcal{I} = \emptyset$ **then**
- 3 Set $\hat{\mathbf{H}} = \mathbf{0}_{n \times (m+1)}$.
- 4 **else**
- 5 Without loss of generality, let $\mathbf{C} = \begin{bmatrix} \mathbf{C}_{\mathcal{I}} \\ \mathbf{C}_{\mathcal{I}^c} \end{bmatrix}$ be the block decomposition of \mathbf{C} into those rows indexed by \mathcal{I} and the relative complement set of rows, $\mathcal{I}^c = [n] \setminus \mathcal{I}$.
- 6 Initialize $t \leftarrow 0$.
- 7 Initialize **error** $\leftarrow \varepsilon + 1$.
- 8 Initialize $\mathbf{H}_{\mathcal{I}}^{(0)} \leftarrow (\mathbf{C}_{\mathcal{I}})_+$.
- 9 **while** **error** $> \varepsilon$ and $t < T$ **do**
- 10 Update $t \leftarrow t + 1$.
- 11 Update $\mathbf{H}_{\mathcal{I}}^{(t)}$ using $\mathbf{H}_{\mathcal{I}}^{(t-1)}$ and $\mathbf{C}_{\mathcal{I}}$ in equation (S28).
- 12 Update **error** $\leftarrow \left\| \mathbf{H}_{\mathcal{I}}^{(t+1)} - \mathbf{H}_{\mathcal{I}}^{(t)} \right\|_{\infty}$
- 13 Again without loss of generality, set $\hat{\mathbf{H}} = \begin{bmatrix} \hat{\mathbf{H}}_{\mathcal{I}} \\ \hat{\mathbf{H}}_{\mathcal{I}^c} \end{bmatrix} = \begin{bmatrix} \hat{\mathbf{H}}_{\mathcal{I}}^{(t-1)} \\ \mathbf{0} \end{bmatrix}$
- 14 Set $\hat{\mathbf{Q}} \leftarrow \hat{\mathbf{Y}} + \hat{\mathbf{H}}\mathbf{A}^{\top}$.

Algorithm 3: Geodesic Second-Order Descent (GSD) Algorithm

Input: Total allowance $\tau > 0$; error tolerance parameter $\varepsilon > 0$; dampening parameter $\alpha > 0$; maximum rotation angle $\theta_{\max} > 0$; “nudge” parameter $\beta > 0$; constraint matrices $\mathbf{B} \in \mathbb{R}^{n \times (m+1)}$ and $\mathbf{A} \in \mathbb{R}^{m \times (m+1)}$; column-centered and column-scaled regressor matrix $\mathbf{X} \in \mathbb{R}^{n \times p}$; empirical quantile functions $\mathbf{Y} \in \mathbb{R}^{n \times m}$; initial allowance vector $\boldsymbol{\lambda}^{(0)} \in \mathbb{R}^p$; maximum iteration count $T \in \mathbb{N}_1$.

Output: Allowance vector $\hat{\boldsymbol{\lambda}}$ solving the sparsity problem (7).

- 1 Initialize $\boldsymbol{\gamma}^{(0)} : \gamma_k^{(0)} = \sqrt{\lambda_k^{(0)} + \beta}$ for each $k = 1, \dots, p$, and normalize $\boldsymbol{\gamma}^{(0)} \leftarrow \sqrt{\tau} \cdot \underline{\boldsymbol{\gamma}}^{(0)}$.
 - 2 Define $\bar{\mathbf{Y}} := n^{-1} \mathbf{1}_{n \times n} \mathbf{Y}$, and define $\tilde{\mathbf{X}} := \mathbf{X} / \sqrt{n}$.
 - 3 Initialize $t \leftarrow 0$.
 - 4 Initialize **error** $= \varepsilon + 1$.
 - 5 **while** **error** $> \varepsilon$ and $t < T$ **do**
 - 6 Update $t \leftarrow t + 1$.
 - 7 Calculate $\mathbf{G} \leftarrow (\tilde{\mathbf{X}} \mathbf{D}_{\boldsymbol{\gamma}^{(t-1)}}^2 \tilde{\mathbf{X}}^\top + \mathbf{I}_n)^{-1}$.
 - 8 Calculate $\hat{\mathbf{Y}} \leftarrow \bar{\mathbf{Y}} + \mathbf{Y} - \mathbf{G} \mathbf{Y}$.
 - 9 Obtain $\hat{\mathbf{H}}$ using Algorithm 2, and active constraint matrix $\mathbf{C} := \text{sign}(\hat{\mathbf{H}})$.
 - 10 Calculate gradient $\nabla g(\boldsymbol{\gamma})$
 - 11 Calculate $\nabla g(\boldsymbol{\gamma}^{(t-1)})$ using equations (S31) and (12).
 - 12 Calculate \mathbf{v} from (15), and calculate $g'_*(0)$ using equation (18).
 - 13 Calculate $g''_*(0)$ using equation (S33).
 - 14 Calculate $\theta_* = \min \left\{ \left| \alpha \cdot \frac{g'_*(0)}{g''_*(0)} \right|, \theta_{\max} \right\}$.
 - 15 Set $\boldsymbol{\gamma}^{(t)} = |\cos(\theta_*) \boldsymbol{\gamma}^{(t-1)} + \sqrt{\tau} \sin(\theta_*) \mathbf{v}|$.
 - 16 Update **error** $= \|\boldsymbol{\gamma}^{(t)} - \boldsymbol{\gamma}^{(t-1)}\|_\infty$.
 - 17 Set $\hat{\boldsymbol{\lambda}} \leftarrow \boldsymbol{\gamma}^{(t)} \circ \boldsymbol{\gamma}^{(t)}$.
-

S6 HYPNOS Data Set

S6.1 List of variables

The dataset used for analysis consisted of $n = 207$ patients which had complete information on $p = 34$ variables collected during the pre-randomization period. These variables comprised:

Demographic variables (4). These included “Age”, “Gender”, “Race_White”, and “Race_Other” (i.e. non-White and non-African American; see Section S6.2).

Baseline health-related variables (5). These included body mass index (“BMI”), point of care “HbA1c”, self-reported average hours of sleep during the work week (“Sleep_Workdays”), Epworth Sleepiness Scale score (“EpworthSS”), and Berlin Questionnaire High/Low OSA risk level (“Berlin”).

Binary medication variables (20). These were coded Yes/No (resp. 1/0), and excluded medications for which < 5 subjects indicated use. The included variables were ACE inhibitor (“ACEI”), alpha adrenergic blocker (“AAB”), angiotensin 2 receptor blocker (“A2RB”), “Anti_Epileptic”, “Aspirin”, “Beta_Blocker”, “Biguanide”, calcium channel blocker (“CCB”), dihydro-calcium channel blocker (“Dihydro_CCB”), glucagon-like peptide-1 receptor agonists (“GLP1RA”), H1 antagonist (“H1_Ant”), “NSAID”, peroxisome proliferator-activated receptor gamma (“PPAR”), proton pump inhibitor (“PPI”), serotonin-norepinephrine reuptake Inhibitor (“SNRI”), selective serotonin reuptake Inhibitor (“SRI”), “Statin”, “Sulfonylurea”, “Thiazide”, and “Thyroxine”.

Oxygen saturation variables (5). These were variables measured during the at-home overnight sleep study, and included mean oxygen saturation (“Mean_Sat”), minimum oxygen saturation (“Min_Sat”), standard deviation of oxygen saturation levels (“Std.Sat”), 4% oxygen desaturation index (“ODI₄”), and proportion of time spent below 90% saturation (“TST90%”).

S6.2 Variable recoding

We coded binary variables as 0/1, with binary Sex label coded as Female = 0, Male = 1. We recoded two other variables as described below.

Oxygen saturation time. One sleep study variable, TST90%, was originally given as the amount of time (in minutes) during the sleep study during which blood oxygen saturation levels were $< 90\%$. Since this time is confounded by the length of the sleep study, which differed from subject to subject, we re-calculated TST90% instead as a proportion of total sleep study time.

Race category. Subject race category was originally coded with values 1 through 6, where 1 corresponded to African American, 2 corresponded to American Indian/Native American, 3 corresponded to Asian or Pacific Islander, 4 corresponded to Caucasian/White, 5 corresponded to Hispanic, and 6 corresponded to Other. Due to small sample sizes in non-White and non-African American categories, we re-coded race into three variables: “Race_White” (1 if race = 4, and 0 otherwise); “Race_Other” (1 if race = 2, 3, 5, 6, and 0 otherwise); and the remaining subjects were identified as African American (race = 1), implicitly defined as the default category, i.e. Race_White = 0 and Race_Other = 0. In total, there were 72 subjects identified as African American, 111 subjects identified as Race_White, and 24 subjects identified as Race_Other.

S6.3 Correlation Analysis

Strong positive or negative correlations between \mathbf{X}_k variables can lead to unstable selection between such correlated variables. During repeated subsampling for stability selection, this instability leads to “vote

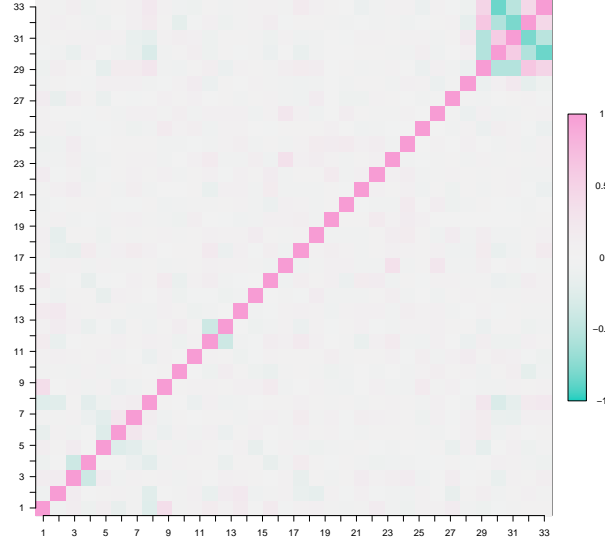


Figure S1: Correlation heatmap of covariates from HYPNOS data. The correlated cluster of five oxygen saturation variables is viewed in the top right of the plot. Small negative correlations at variables 3 and 4 correspond to indicators for self-reported race category (Race_White, and Race_Other, respectively), and small negative correlations at 11 and 12 correspond to two hypertension drugs (A2RB and ACEI, respectively), which are not co-prescribed.

splitting” between correlated variables, such that no variable’s empirical selection probability is high, i.e. exceeds threshold π_{thr} . Correlation analysis of HYPNOS data reveals the sleep study oxygen saturation variables have strong negative and positive correlations among themselves, forming a correlated cluster of 5 variables.

We provide visualizations of this cluster in two ways. First, Figure S1 shows (signed) Pearson correlations between all variables \mathbf{X}_k , with the oxygen variables taking the last five places in the variable ordering. The correlation plot shows strong positive and negative correlations between all oxygen saturation variables, with all pairwise correlations ≥ 0.44 and each variable having at least one pairwise correlation ≥ 0.6 . By contrast, the largest magnitude pairwise correlation outside of this cluster is < 0.4 . Second, Figure S2 illustrates the oxygen saturation cluster by column-clustered dendrogram, using similarity metric $1 - |\text{cor}(\mathbf{X}_j, \mathbf{X}_k)|$. The first split of the full variable set from the dendrogram “root” is between the oxygen saturation variables (left-most group) and the other variables.

To circumvent the correlation problem, we perform principal component analysis on the 5 oxygen saturation variables, obtaining orthogonal principal components (PCs) which we use in place of the original 5 variables. Table S1 gives the loadings associated with the 5 PCs. Since our data analysis shows the 2nd PC is selected, Figure S3 illustrates pairwise scatterplots of the original oxygen variables, colored by value of this PC.

S6.4 Effects Interpretation

Three variables of the $p = 34$ HYPNOS data set were selected by applying an “any vote” procedure on the complementary pairs stability selection “stability paths” from Shah and Samworth (2013): HbA1c, a binary indicator for sulfonylurea use, and the 2nd oxygen principal component (Section S6.3). Three

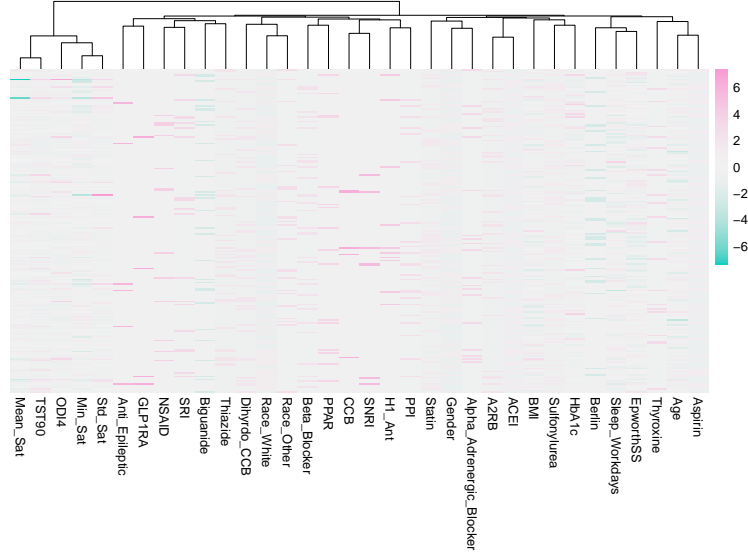


Figure S2: Dendrogram and correlation plot of \mathbf{X}_k variables from HYPNOS data set, using $1 - |\text{cor}(\mathbf{X}_j, \mathbf{X}_k)|$. The five oxygen variables are grouped together, on the left of the graphic.

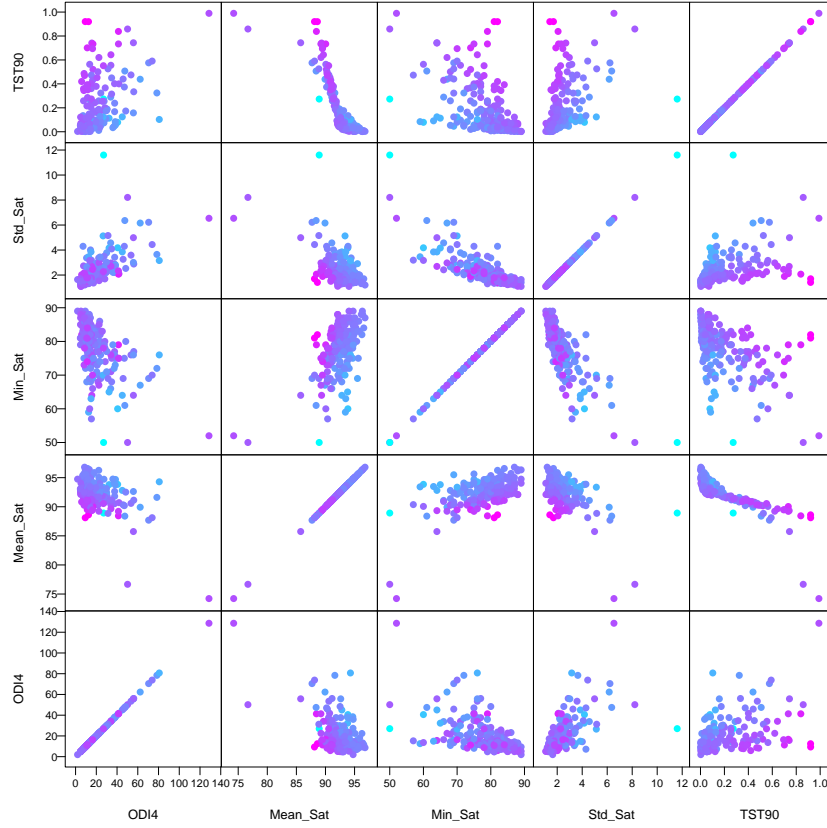


Figure S3: Pairwise scatterplots of oxygen saturation variables, with color scale according to $\text{PC}_{2,\text{oxygen}}$ value.

Variable	PC_1	PC_2	PC_3	PC_4	PC_5
ODI ₄	−0.419	−0.242	−0.850	−0.208	0.001
Mean_Sat	0.470	−0.462	−0.024	−0.314	−0.683
Min_Sat	0.455	0.360	−0.480	0.626	−0.202
Std_Sat	−0.455	−0.477	0.198	0.660	−0.301
TST90	−0.436	0.609	0.083	−0.174	−0.634

Table S1: PCA loadings on oxygen saturation variables.

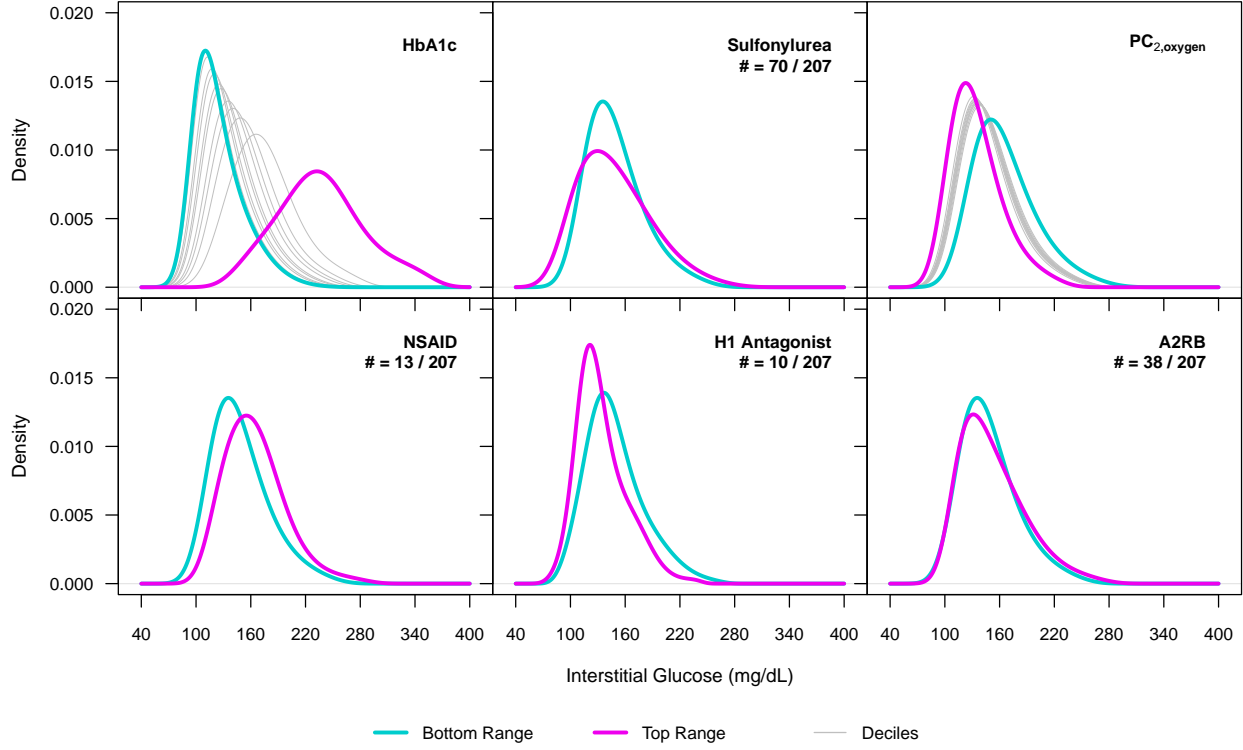


Figure S4: Predicted densities using Fréchet regression with 6 variables, including 3 selected variables (*top row*) and 3 nearest non-selected variables (*bottom row*). In each panel, the levels of the corresponding covariate are varied from the lowest/“no” (bottom range, cyan) to the highest/“yes” (top range, magenta). Grey lines correspond to evaluations at 0.1 decile changes in corresponding variable. The remaining variables are kept constant, at sample mean for HbA1c, “no” for medication use variables, and zero for $PC_{2,oxygen}$.

variables’ stability paths were marginally close to the selection threshold (i.e. had $\hat{\Pi}_B(k; \tau)$ within 0.1 of $\pi_{thr}(\tau)$ for some τ), namely, indicators for use of non-steroidal anti-inflammatory drugs (NSAIDs), use of H1 antagonists (an antihistamine family), and use of angiotensin 2 receptor blockers (A2RBs, a family of hypertension medications). To ascertain whether inclusion of these variables in the selected variable set affects our effects interpretations of the three selected variables, we replicate the marginal effects analysis while including the three new medication use variables; the results are illustrated in Figure S4. For ease of comparison, we repeat the original marginal effects plot in Figure S5.

The marginal changes in glucose mean and standard deviation from high to low input variable values, comparing the 3-variable and 6-variable models, are given in Table S2. Including the extra three medication use variables results in only a small change in the estimated effect across the empirical range of input values.

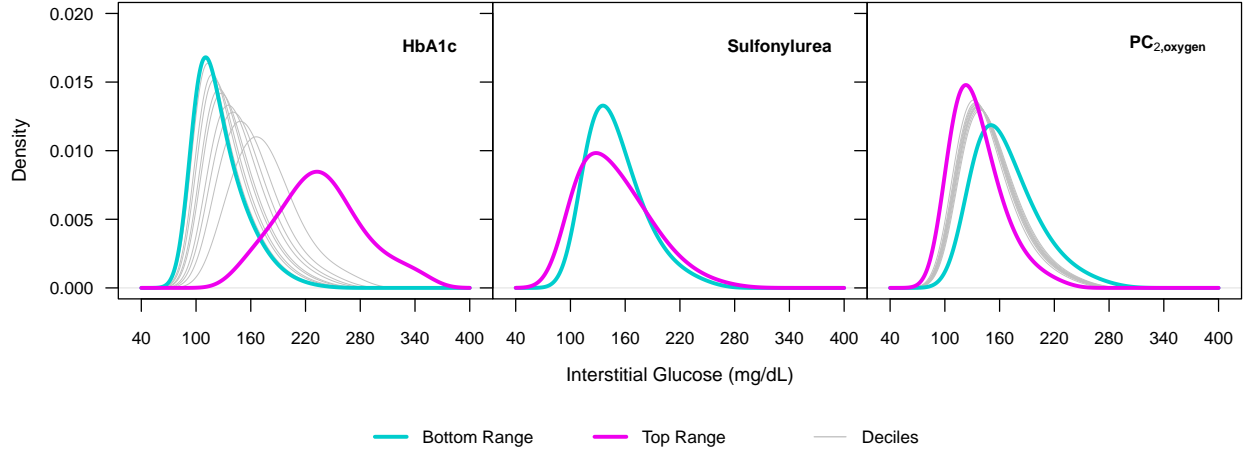


Figure S5: Predicted densities using Fréchet regression with 3 selected variables. In each panel, the levels of the corresponding covariate are varied from the lowest/“no” (bottom range, cyan) to the highest/“yes” (top range, magenta). Grey lines correspond to evaluations at 0.1 decile changes in corresponding variable. The remaining variables are kept constant, at sample mean for HbA1c, “no” for sulfonylurea use, and zero for $PC_{2,oxygen}$.

Model	Variable	Change in glucose over empirical range	
		Mean	SD
3-Variable	HbA1c	126.2 → 236.7 (+110.5)	28.9 → 49.2 (+20.3)
	Sulfonylurea	150.0 → 149.3 (−0.7)	33.2 → 42.1 (+8.9)
	PC_{2,oxygen}	167.3 → 135.5 (−31.8)	37.1 → 29.9 (−7.2)
6-Variable	HbA1c	124.7 → 236.8 (+112.1)	28.1 → 49.4 (+21.2)
	Sulfonylurea	148.8 → 148.7 (−0.1)	32.6 → 41.5 (+8.9)
	PC_{2,oxygen}	165.6 → 134.7 (−30.8)	36.1 → 29.7 (−6.3)
	NSAID	148.8 → 164.5 (+15.7)	32.6 → 34.3 (+1.7)
	H1 Antagonist	148.8 → 134.4 (−14.4)	32.6 → 28.2 (−4.4)
	A2RB	148.8 → 152.6 (+3.8)	32.6 → 36.5 (+3.9)

Table S2: Marginal effects on glucose levels across full empirical range of given input variables (i.e. minimum → maximum for numeric variables, and “no” → “yes” for binary variables). Top three rows show marginal changes for the model consisting of selected variable set only (Section 7); bottom six rows show marginal changes for the model also including next-three closest variables to selection threshold. Selected variable rows are bolded. For min-max comparison of a single variable, all other inputs are set to constant levels: empirical mean value for numeric variables, and “no” for binary variables.

We do note the range of $PC_{2,oxygen}$ values in the HYPNOS data set might not be a representative description of input range for this principal component, e.g. there is larger separation between the top/bottom range marginal curves in the $PC_{2,oxygen}$ panels of Figures S5 and S4 and the decile curves. For completeness, we also present marginal effects between the empirical 2.5% and 97.5% $PC_{2,oxygen}$ quantiles, i.e. across the “central” 95% range, in Table S3. In contrast to a mean change of -31.8 mg/dL and SD change of -7.2 mg/dL over the full range, the mean and SD change over the central 95% range are -14.8 and -3.4 mg/dL, respectively, in the 3-variable model.

Model	Variable	Change in glucose over 2.5 \rightarrow 97.5% range	
		Mean	SD
3-Variable	PC _{2,oxygen}	157.8 \rightarrow 143.0 (−14.8)	35.0 \rightarrow 31.6 (−3.4)
6-Variable	PC _{2,oxygen}	156.3 \rightarrow 142.0 (−14.3)	34.2 \rightarrow 31.2 (−2.9)

Table S3: Marginal effects on glucose levels across central empirical 95% range of PC_{2,oxygen} values, using same models as in Table S2. All other inputs are set to constant levels: empirical mean value for numeric variables, and “no” for binary variables.